DEVELOPMENT OF AN OPTICAL DISSOLVED OXYGEN SENSOR

By

ANTOINETTE SHIELDS, B.Sc.

Submitted for the Degree of

MASTER OF SCIENCE

Presented to

DUBLIN CITY UNIVERSITY

Research Supervisor:

DR. COLETTE McDONAGH,
School of Physical Sciences,
Dublin City University.

AUGUST 1999

Declaration:

I hereby certify that this material, which I now submit for the assessment on the programme of study leading to award of M.Sc. in Applied Physics, is entirely my own work and has not been taken from the work of others save and to the extent that such work has been cited and acknowledged within the text of my work.

Signed: Antoinette Shields Date: 13/9/99

Dedication

To Mam and Dad

Acknowledgements:

I would like to thank the following people for their help throughout this project:

- To Colette, for her advice, encouragement and eternal optimism – it was very much appreciated.
- To Brian, for his support and enthusiasm and also to the industrial sponsors of this project Severn Trent Water Ltd.
- To Alan Hughes, for the technical expertise and never-ending enthusiasm. Also to the guys at PEI, Kevin and Liam for all the hard work.
- To past and present members of the Optical Sensors Lab., in particular fellow member of the girlie lab, Penny, and also to Aidan, Colm and Paud for brightening many a dull day! Also, thanks to Sarah-Jane for tolerating the constant interruptions.
- A special word of thanks to my two friends and partners in crime, Tobi and Jeff.
- Finally, to my family, in particular, my parents Margaret and Gerry and also Ann, Gerard, and Claire, for their support and encouragement over the years.

Abstract

A dissolved oxygen sensor based on fluorescence quenching of the oxygen-sensitive ruthenium complex, [Ru(II)-tris(4,7-diphenyl-1,10-phenanthroline]$^{2+}$, which has been immobilised in a porous silica sol-gel-derived film, is reported. Ormosil sensing films are fabricated using the modified silica precursors methyltriethoxysilane (MTEOS) and ethyltriethoxysilane (ETEOS), and are dip-coated onto planar glass substrates. Due to their increased hydrophobicity compared with conventional sol-gel precursors, such as tetraethoxysilane (TEOS), the use of these modified precursors enables the fabrication of the optimum sensor films for the purposes of dissolved oxygen sensing.

This project aims to investigate a number of issues that have been identified as being of crucial importance for optimum sensor performance. In particular, the long-term stability of the sensor films is investigated and issues such as dye leaching and photobleaching are discussed. The development and optimisation of a suitable barrier layer for the purpose of optical isolation of the sensor films is also detailed. Additionally, an investigation to establish the temperature dependence of the sensor is reported. Finally, the progress towards a commercial instrument is documented.

Table of Contents:

Chapter 1: Introduction

1.1: Introduction

Oxygen is an immensely important chemical species, vital for life. The intimate involvement of oxygen in the life processes of photosynthesis and respiration has induced the need to determine its concentration in a variety of environments for scientific or technological purposes. In many aqueous environments it is necessary to know the dissolved oxygen level to ensure a healthy environment for flora and fauna. On the other hand, the measurement of oxygen is a vital diagnostic tool in medicine, or it is simply a question of sound economics such as in the food processing industry. However, the need for *in situ* measurements or continuous monitoring of oxygen levels has placed demands on conventional methods, with which they are unable to cope. The necessity for an oxygen sensor that is fast, reliable and that can be easily adapted for any number of applications has prompted considerable research in this field. The recent advances in the area of optical oxygen sensors have produced instruments that match these requirements.

This project is concerned with the development and characterisation of an optical dissolved oxygen sensor. A porous sol-gel derived glass is doped with a ruthenium complex whose fluorescence is quenched in the presence of oxygen. Characterisation and optimisation of the sensor performance was carried out with a view to the development of a commercial instrument.

1.2: Dissolved Oxygen

Pure water, free from any dissolved substances does not exist outside the laboratory. All natural water contains dissolved gases and salts, of which oxygen is undoubtedly the most important, since it sustains the life in these waters. The actual amount of dissolved oxygen (DO) present in the cleanest water is extremely small, although it is entirely adequate to support the fauna and flora of an unpolluted river. At a temperature of 20°C, the solubility of oxygen in water is 9.2 milligrams per litre (9.2mg/L) which is approximately 9 parts per million (9ppm). Any increase in the temperature of the water results in a decrease in the solubility of the oxygen as shown in figure 1.1 [1].

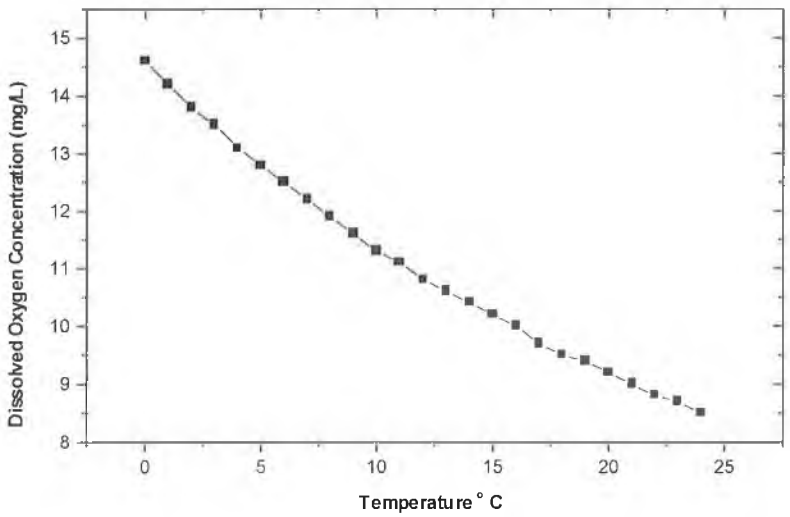

Figure 1.1: Dissolved oxygen concentration as a function of temperature. (Oxygen concentrations in mg/L corresponding to 100% saturation.)

An unpolluted river with an oxygen level of around 9ppm will have a healthy flora and fauna, which will include a substantial population of aerobic bacteria. The numbers of these bacteria are limited by the absence of suitable food, i.e., digestible organic matter. The level of dissolved oxygen in this river is never static but instead remains in a state of dynamic equilibrium, with the balance maintained by biochemical depletion and continued reoxygenation [2]. However, if a sufficiently large quantity of waste is discharged into the river, the rate of bacterial uptake of the dissolved oxygen will outstrip that at which the DO is replenished from the atmosphere and from photosynthesis. The bacterial degradation of the waste continues as the DO levels fall further. Anaerobic conditions now prevail resulting in the production of the foul-smelling hydrogen sulphide and substantial fish deaths.

Similarly in sewage treatment plants, the biochemical breakdown of the waste is achieved by bacterial attack in the presence of oxygen. A lack of sufficient air in this process results in the increased activity of anaerobic, sulphate-reducing bacteria, and the production of hydrogen sulphide, causing costly corrosion problems. However, aeration of the waste is the largest single operating expense and oxygen levels surplus to requirements prove to be wasteful and inefficient.

It is apparent that constant monitoring of dissolved oxygen levels is required in these two cases to ensure a careful balance is maintained. Indeed, successful dissolved oxygen monitoring is vital in many areas, not least in the environmental control of natural waters and for sewage and wastewater treatment, but also for medical and biochemical studies, and for food and drug process control. Hence a need exists for an efficient, reliable method of measuring dissolved oxygen, which can be adapted easily to suit any environment.

There are two methods widely used for the measurement of dissolved oxygen. The first is the Winkler method, which is the most precise and reliable titrimetric procedure for DO analysis, and the second is the amperometric Clarke electrode method, based on the reduction of oxygen at an electrode after diffusion across an oxygen permeable membrane [2]. These methods are commonly used today and often yield good results although they do have a number of drawbacks associated with them.

The Winkler method is time consuming and can yield misleading results due to lack of care and precision in methodology. This method is not suitable for *in situ* measurements or for continuous monitoring. The Clarke electrode has a slow response time and consumes oxygen during the measurement.

It has been proposed that optical oxygen sensors would prove to be a very suitable alternative to these conventional methods. Optical sensors use variations in light to detect certain analytes, and offer a number of advantages as discussed in the next section and in subsequent chapters.

1.3: Optical Sensors

A sensor is a device that measures a physical parameter or the concentration of a particular analyte. Optical sensors achieve this by measuring changes in optical signals as a function of the measurand. In general, optical sensors offer a number of advantages over conventional sensing methods. Most importantly perhaps is the fact they are cost-effective to produce, easy to use, and also easily miniaturised. Additionally, they do not suffer from electrical interference, and are compatible with the vast range of optoelectronic devices such as LED's and photodiodes currently available.

Given these advantages and also the widespread importance of the quantitative determination of oxygen, it is not surprising that much research has been carried out into the development of optical oxygen sensors [3,4,5]. In particular, fluorescence based sensors have proved very promising due to their high selectivity and sensitivity. They can also be used for continuous monitoring or *in situ* measurements. The principle of operation of these sensors is based on the fluorescence quenching by molecular oxygen of a suitable dye complex immobilised in a porous support matrix. An important feature of this type of sensor is the fact that no oxygen is consumed during the process and it is entirely reversible. This facet of the fluorescence based oxygen sensors coupled with their fast response times makes them a more attractive choice than the more conventional methods such as the Winkler method or the Clarke electrode.

1.4: Sol-Gel Thin Films

The sol-gel process is a low-temperature method of fabricating porous glass. The process enables the production of fibres, monoliths, and also thin films [6]. These thin films are easily prepared by dip-, spin-, or spray-coating the liquid sol onto the required substrate. The resulting coatings are thermally stable, chemically inert, and intrinsically bound to the substrate, making them very suitable for use as support matrices for sensor molecules.

Detailed information regarding the sol-gel process is provided in Chapter 2. However, in short, the process entails the addition of the chosen dye complex to a liquid silicon alkoxide precursor, which undergoes both hydrolysis and condensation reactions and forms a solid.

The resulting cage-like structure physically entraps the sensor molecules, although the smaller analyte molecules such as oxygen can permeate the matrix and access the dye complex in the pores. Variation of the initial fabrication parameters enables tailoring of the film microstructure for a variety of sensing applications [7].

Considerable work has already been done in this area [8,9,10,11]. This laboratory alone has reported the use of sol-gel thin films for a variety of sensing applications including the detection of gas-phase oxygen, dissolved oxygen, ammonia and pH measurement [12,13,14].

1.5: Sensor Configurations

Sol-gel immobilisation as outlined in chapter 2 facilitates the development of a diverse range sensor configurations. Colleagues carrying out research in the area of optical sensors at Dublin City University have developed a number of different configurations. Perhaps the most prevalent of these are the waveguide methods, consisting of a sol-gel coating deposited on an optical fibre, to produce intrinsic evanescent-wave sensors for the measurement of oxygen concentration or pH. Both phase-fluorimetric-based [15] and intensity-based configurations [12] have been implemented. Planar waveguides are also used. Much work has been done in this area by Doyle *et al* who have implemented a variety of planar waveguide configurations for a number of different sensing applications, among them the sensing of ammonia, oxygen and the measurement of pH [16]. More recently, a novel technique was developed by Gouin *et al*, based on the capture of fluorescence by a planar waveguide [17]. This method offers the attractive option of a filter-free optical sensor. Alternatively, the configuration relevant to this work is the direct excitation of sol-gel coated planar glass substrates. Further details regarding the experimental system used in this work are provided in chapter 4.

1.6: Objectives of the Project

The principal objectives of this work were:

(1.) Investigation of the long-term stability of the doped sol-gel films, in particular with regard to leaching and photobleaching of the incorporated dye complex.

(2.) Fabrication and characterisation of an effective optical isolation layer.

(3.) Investigation of the temperature dependence of the dissolved oxygen sensor.

(4.) Design and implementation of a prototype dissolved oxygen sensor suitable for field-testing.

These objectives will be revisited in chapter 9 with respect to the level of achievement of these aims.

References

[1.] P. J. Flanagan; **Parameters of Water Quality: Interpretation and Standards**, Environmental Research Unit, 1988.

[2.] M. L. Hitchman; **Measurement of Dissolved Oxygen**, John Wiley, Geneva, 1978.

[3.] O. S. Wolfbeis; **Fiber Optic Chemical Sensors**, **Vol.** II, CRC Press, 1991.

[4.] A. Mills; **Optical Oxygen Sensors: Utilising the luminescence of platinum metal complexes**, *Platinum Metals Rev.,* 1997, Vol. 41, no. 3, pp. 115-127.

[5.] A. K. McEvoy; **Development of an Optical Sol-Gel-Based Dissolved Oxygen Sensor**, PhD Thesis, 1996, Dublin City University, (unpublished).

[6.] L. C. Klein; **Sol-Gel Glass Technology: A Review**, *Glass Ind.*, 1981, Vol. 14, pp. 17.

[7.] C. J. Brinker, G. W. Scherer; **Sol-Gel Science: The Physics and Chemistry of Sol-Gel Processing**, Academic Press, San Diego, 1990

[8.] S. C. Kraus, R. Czolk, J. Reichert, H. J. Ache; **Optimization of the sol-gel process for the development of optochemical sensors**, *Sensors and Actuators B,* 1993, Vol. 15-16, pp. 199-202.

[9.] A. Wilson, J. D. Wright, J. J. Murphy, M. A. M. Stroud, S. C. Thorpe; **Sol-Gel materials for gas-sensing applications**, *Sensors and Actuators B,* 1994, Vol. 18-19, pp. 500-510.

[10.] N. Aharonson, M. Altstein, G. Avidan, D. Avnir, *et al.*; **Recent developments in organically doped sol-gel sensors: A microns scale probe**, *Mat. Res. Soc. Symp. Proc.*, 1994, Vol. 346, pp. 519-530.

[11.] P. Lavin; **Optimisation of Ormosil Thin Films for Sensor Applications**, MSc. Thesis, 1997, Dublin City University, (unpublished).

[12.] B. D. MacCraith, C. M. McDonagh, G. O'Keeffe, A. K. McEvoy, T. Butler, F. R. Sheridan; **Sol-Gel coatings for optical chemical sensors and biosensors**, *Sensors and Actuators B*, 1995, Vol. 29, pp. 51-57.

[13.] C. M. McDonagh, B. D. MacCraith, A. K. McEvoy; **Tailoring of sol-gel films for optical sensing of oxygen in gas and aqueous phase**, *Anal. Chem.*, 1998, Vol. 70, no. 1, pp. 45-50.

[14.] A. Doyle, B. D. MacCraith; **Fabrication of sol-gel based planar waveguide/grating coupler platforms for use as optical chemical sensors**, *Proc. SPIE,* 1997, Vol. 3105, pp. 61-70.

[15.] G. O'Keefe, B. D. MacCraith, A. K. McEvoy, C. M. McDonagh; **Development of a LED-based phase fluorimetric oxygen sensor using evanescent-wave excitation of a sol-gel immobilized dye**, *Sensors and Actuators B,* 1995, Vol. 29, pp. 226-230.

[16.] A. Doyle, **Development of Optical Sensor Platforms based on Evanescent Wave Interactions**, PhD Thesis, 1999, Dublin City University, (unpublished).

[17.] J. F. Gouin, A. Doyle, B. D. MacCraith; **Fluorescence capture by planar waveguide as platform for optical sensors,** *Electronics Letters,* 1998, Vol. 34, no. 17, pp. 1685-1687.

Chapter 2: The Sol-Gel Process and Thin Film Fabrication

2.1: Introduction

The sol-gel process is a low temperature method of producing glass either as thin films or monoliths. The success of this method is primarily due to its ability to form pure and homogenous products at low temperatures. It involves the hydrolysis and condensation of an alkoxide precursor in the presence of water, a catalyst, and a solvent [1]. The detailed microstructure of sol-gel glasses is dependent on a large number of processing parameters and hence one of the distinctive features of the sol-gel process is that the properties of any films derived from this method may be tailored by adjusting these parameters during fabrication [2].

The following chapter explores many of the facets of sol-gel science. Details of the chemistry of the reactions and the various fabrication parameters involved in the process are documented. Information is also provided on the formation of thin films, in this case used for the purposes of sensor fabrication.

2.2: The Sol-Gel Process

For silica glasses, the sol-gel process involves the hydrolysis and condensation of silicon alkoxide precursors. A precursor is a compound consisting of a metal surrounded by various ligands. The silicon alkoxide precursors have the general formula $Si(OR)_4$. One of the most widely used of these metal precursors is tetraethoxysilane (TEOS). In this case silicon is the central metal atom which is surrounded by four ethoxy groups and the chemical formula is $Si(OC_2H_5)_4$.

Initially the precursor is mixed with water. A mutual solvent such as alcohol is generally required as a homogenising agent, because water and silicon alkoxides are immiscible. It must be noted however that the added alcohol is not essential since the hydrolysis reaction will generate sufficient alcohol.

After mixing, the hydrolysis and condensation reactions are left to proceed for a period known as the ageing time. This can be carried out at room temperatures or higher if required. Consequently, the sol is viscous enough for further processing. A schematic of the overall sol-gel process is shown in figure 2.1.

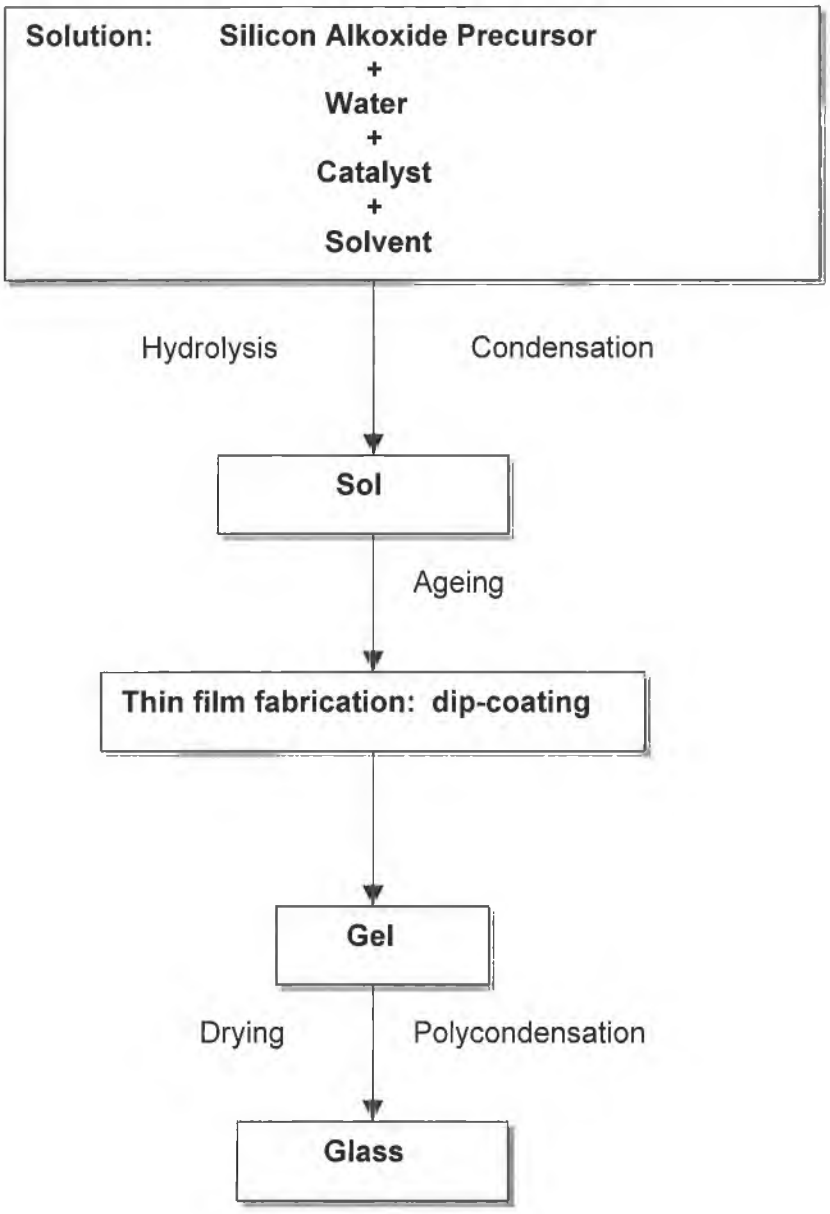

Figure 2.1: The sol-gel process.

2.2.1: Hydrolysis and Condensation

The sol-gel process is characterised by two basic reactions namely, the hydrolysis and condensation of various precursors dissolved in alcohol in the presence of some water, with either an acid or base catalyst. For silica glass the silicon alkoxide precursor is hydrolysed by mixing with water. The hydrolysis involves the nucleophilic attack by the oxygen in the water on the silicon atom, resulting in the replacement of the alkoxide groups (OR) with the hydroxyl groups (OH).

$$\text{Hydrolysis:} \quad \equiv Si - OR + H_2O \Leftrightarrow \equiv Si - OH + ROH \qquad (2.1)$$

The condensation reactions involve the silanol groups (OH^-). Nucleophilic condensation reactions result in the production of siloxane bonds, ≡Si–O–Si≡. These reactions often begin before the completion of the above hydrolysis reaction, and also yield by-products of alcohol (ROH) and water. A three-dimensional Si-O-Si network is built up as a result of the condensation processes.

$$\text{Water Condensation:} \quad \equiv Si - OH + HO - Si \equiv \Leftrightarrow \equiv Si - O - Si \equiv + H_2O \qquad (2.2)$$

$$\text{Alcohol Condensation:} \quad \equiv Si - OR + HO - Si \equiv \Leftrightarrow \equiv Si - O - Si \equiv + ROH \qquad (2.3)$$

2.3: Sol-Gel Processing Parameters

The material properties of the sol are influenced by the various processing parameters involved in its fabrication. These parameters include the water to precursor ratio, the sol pH, the ageing time and temperature, and the catalyst type used [4]. These variables affect the hydrolysis and condensation rates, the evolving microstructure of the sol, and the resulting solid structure.

2.3.1: Water to Precursor Ratio (R value)

At any given pH value, the structure of the sol-gel silicates evolves as a result of the rates of the hydrolysis and condensation reactions. The molar ratio of water to precursor present in the initial sol is called the R value. An increase in this value (i.e. an increase in the amount of water present) results in an increase in the relative rates of hydrolysis and condensation. In theory, an R value of 2 is sufficient for complete hydrolysis [3].

However, often due to the presence of intermediate species, and the occurrence of reverse reactions such as esterification and alcoholysis, R=2 proves inadequate.

Generally, an increase of the R value in the limit of low pH, decreases the gel time of a sol, thereby providing a more viscous sol which will in turn produce a thicker coating film. However it must be noted that beyond a certain R value the excess water serves only to dilute the sol, decreasing the film thickness [5]. An important feature of R=2 films which is relevant to this project, is their large average pore size compared to that for R=4 films. This is consistent with a slightly denser, more cross-linked microstructure for R=4 films, resulting from the faster hydrolysis and condensation rates [6,7].

2.3.2: Sol pH

The rates of both the hydrolysis and condensation reactions are dependent upon the pH of the starting solution. At the isoelectric point the surface charge is zero, and for silica this occurs at pH of 2. This pH forms the boundary between acid catalysis (pH<2) of the process and base catalysis (pH>2) [3]. Acid catalysis results in fast hydrolysis rates and relatively long gel times. The resulting gel consists of a network structure of linear chains with a fine microporous structure. Alternatively, base catalysis is associated with slow hydrolysis rates, faster condensation rates and hence shorter gel times. Under these conditions, more dense colloidal particles are formed, resulting in larger average pore size compared with acid catalysed gels.

2.3.3: Ageing Time

The ageing time is the period after mixing during which both the hydrolysis and condensation reactions are allowed to proceed. Throughout this period, the sol is allowed to stand either at room temperature or at a higher temperature. Effectively, this produces a viscous sol suitable for use in the fabrication of thin sensing films.

2.4: Thin Film Fabrication

One of the most significant aspects of the sol-gel process lies in the fact that prior to gelation the sol is ideal for the deposition of thin films. Despite the presence of a whole range of techniques for producing optical thin films [8], both spin-coating and dip-coating remain the most extensively used [9, 10]. Spin coating is achieved by depositing a few drops of the sol on the surface of the substrate. Then, as the name suggests the substrate is spun around to produce the film [11]. However, despite the advantage of there being little waste, this coating method is not suitable for non-circular substrates. Hence the dip coating method was deemed a more satisfactory choice for the purposes of this work.

2.4.1: Dip Coating

The primary advantage of the dip coating technique is that a substrate of any shape or size may be coated effectively. Also, the apparatus required is generally inexpensive and relatively simple. The computer-controlled dip coating apparatus used for sensor fabrication during the course of this work for is shown in figure 2.2.

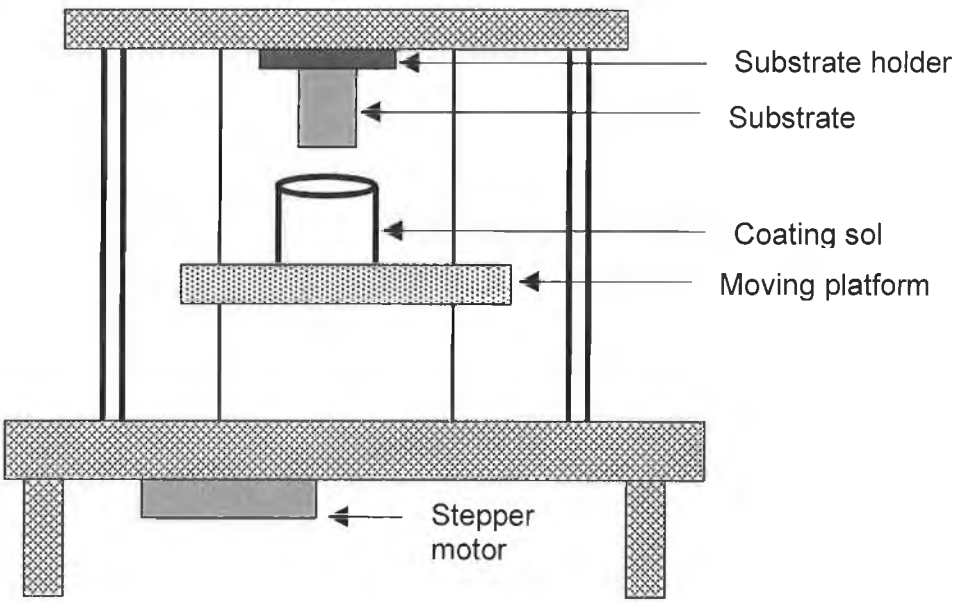

Figure 2.2: Computer controlled dip-coating apparatus.

During the process, the sample is held rigid and the sol is held on a moving platform. Initially, the substrate is lowered into the sol by moving the platform containing the reservoir of sol in an upward direction. When sufficiently immersed the substrate is withdrawn at a constant velocity, again by moving the platform containing the reservoir, this time in a downward direction allowing deposition of the sol. After coating, the sample must remain undisturbed to allow it to equilibrate. Flow from the top to the bottom of the substrate continues. As long as the newly coated substrate remains undisturbed in a draught and vibration free environment, an even film should form, with only a small uneven deposit at the bottom of the slide.

Certain factors affect the thickness of the film deposited on the substrate [12]. Among them is the dipping speed [5]. For this work, all films were dipped at a constant withdrawal speed of 1mm/sec.

2.4.2: Substrate Preparation

The use of clean substrates for film deposition is vital. This ensures the production of good quality, uniform films. Hence, all surfaces to be coated should be even, preferably polished, with all dirt and dust removed prior to deposition.

For this project, planar glass substrates were prepared by cutting soda-lime microscope slides into quarters. These glass slides were then cleaned thoroughly by washing with deionised water, methanol, acetone, and finally deionised water again. The slides were then placed into a container of deionised water, which was put into an oven at 70°C for 24 hours. This is thought to condition the slides by increasing the number of surface silanol groups and hence improve the adhesion of the sol-gel film to the substrate.

2.4.3: Drying Time

After the deposition of the sol onto the substrate the sensing films are placed into the oven at 70°C for 18 hours. This is known as the drying time. This drying serves to remove excess fluid in the films [3].

2.5: Ormosils

The most common silicon precursor used in sol-gel work is tetraethoxysilane (TEOS). This precursor was used in the early stages of sensor development in this laboratory [13]. More recently, and for the purposes of this project, *or*ganically *mo*dified *sil*anes, or ormosils have been used. An example of this type of precursor is methyltriethoxysilane or MTEOS, which was the primary precursor used during the course of this work. ETEOS or ethyltriethoxysilane was also used. As before, these compounds consist of a central metal ion (silicon) which is again surrounded by ligands, but in this case one or more of the ligands is an organic group such as a methyl or ethyl group. These compounds proffer a number of advantages when used for sensor fabrication, the most important of which is increased hydrophobicity which will be detailed further in chapter 4.

2.6: Sensor Dye Incorporation

In optical sensor work the use of various dye molecules to sense for various analytes is widespread as discussed in Chapter 1. The choice of a suitable host matrix for these dyes is important for the effective operation of these sensors. The matrix must fully support the dye complex, and allow easy access by the analyte to the dye.

Sol-gel glass is thought to be a very suitable host matrix. Dye complexes are easily incorporated during fabrication of the sol-gel without any damage to the complex. It is believed that the sol-gel structure forms around the dye complex ensuring it is physically entrapped in the porous silica structure. Careful tailoring of the fabrication parameters of the sol-gel controls the pore size of the glass as discussed. Larger pore sizes enable full accessibility by the analyte to the dye complex, although care must be taken to ensure leaching of the dye is not a problem. A balance in pore size must be reached whereby any leaching of the dye is minimised but the dye remains accessible to the analyte via the pores. This issue is investigated further in chapter 5.

The oxygen sensitive dye chosen for this project was Ru(II) tris(4, 7-diphenyl-1, 10-phenanthroline) or $[Ru(Ph_2phen)_3]^{2+}$. Further details regarding this compound are provided in chapter 3.

2.7: Summary

The sol-gel process has proved particularly useful and versatile for the production of sensor platforms. The chemistry of this process was documented in this chapter. Details of the various fabrication parameters and the effect of altering these parameters were provided. The methods of thin film fabrication and the apparatus used throughout this work for this purpose were also described in this chapter.

References

[1.] L. L. Hench, J. K. West; **The Sol-Gel Process**, *Chem. Rev.*, 1990, Vol. 90, pp. 33-72.

[2.] S. Sakka; **The Current State of Sol-Gel Technology**, *J. Sol-Gel Sci. Technol.*, 1994, Vol. 3, pp. 69-81.

[3.] C. J. Brinker, G. W. Scherer; **Sol-Gel Science: The Physics and Chemistry of Sol-Gel Processing**, Academic Press, San Diego, 1990.

[4.] C. McDonagh, F. R. Sheridan, T. Butler, B. D. MacCraith; **Characterisation of sol-gel derived silica films**, *J. Non-Crys. Solids*, 1996, Vol. 194, pp. 72-74.

[5.] F. R. Sheridan; **Characterisation and optimisation of sol-gel-derived silica coatings for use in optical sensing**, M.Sc. thesis, Dublin City University, 1995.

[6.] A. K. McEvoy; **Development of an Optical Sol-Gel-Based Dissolved Oxygen Sensor**, PhD Thesis, 1996, Dublin City University, (unpublished).

[7.] T. M. Butler; **Development of Evanescent Wave pH Sensors Based on Coated Optical Fibres**, PhD Thesis, 1996, Dublin City University, (unpublished).

[8.] P. Marage, M. Langlet, J. C. Joubert; **A new route for the deposition of SiO_2 sol-gel coatings**, *Thin Solid Films*, 1994, Vol. 238, pp. 218-277.

[9.] R. M. Almeida; Sol-**Gel silica films on silicon substrates**, *International Journal of Optoelectronics*, 1994, Vol. 9, no. 2 pp. 135-142.

[10.] C. J. Brinker, A. J. Hurd, P. R. Schunk, G. C. Frye, C. S. Ashley; **Review of sol-gel thin film formation**, *J. Non-Crys. Solids*, 1992, Vol. 147&148, pp. 424-436.

[11.] I. M. Thomas; **Optical Coating Fabrication**, *Sol-Gel Optics: Processing and Applications*, Kluwer Academic Publishers, 1994, pp. 141-158.

[12.] I. Strawbridge, P. F. James; **The factors affecting the thickness of sol-gel derived silica coatings prepared by dipping**, *J. Non-Crys. Solids*, 1986, Vol. 86 pp. 381.

[13.] A. K. McEvoy, C. McDonagh, B. D. MacCraith; **Dissolved oxygen sensor based on fluorescence quenching of oxygen-sensitive ruthenium complexes immobilized in sol-gel derived porous silica coatings,** *The Analyst,* 1996, Vol. 121, pp. 785-788.

Chapter 3: Oxygen Sensing by Fluorescence Quenching

3.1: Introduction

The following chapter discusses the principle of operation of the dissolved oxygen sensor used throughout this work, namely, the quenching by oxygen of a fluorescent ruthenium complex entrapped within a sol-gel matrix. The concepts of fluorescence and collisional quenching are introduced and explained, and the properties of the ruthenium complex used are documented.

3.2: Fluorescence

Fluorescence is the emission of a photon of light from an atom or molecule, resulting from the de-excitation of an electron from an excited state to a ground state energy level. The details of this process are illustrated schematically in Figure 3.1.

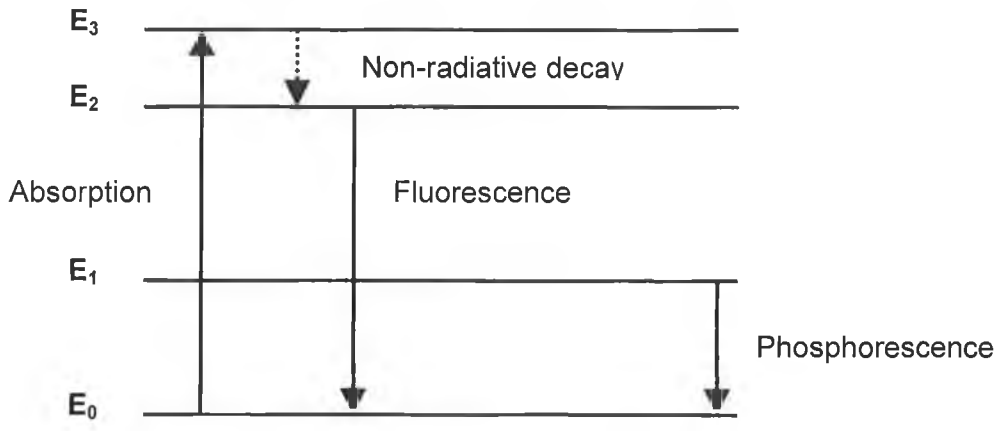

Figure 3.1: Schematic of basic excitation and emission processes.

In a molecule, every electron possesses a spin angular momentum with a spin quantum number, s=1/2. The electron can be either 'spin-up' or 'spin-down', denoted by the use of the arrows, ↑ or ↓. In a many-electron atom or molecule, the total spin angular momentum is represented by the total spin quantum number (S), which may be calculated from the vector sum of the individual contributions from each electron [1]. In the case of two electrons with opposing spins, the total spin quantum number, S, is zero. Alternatively, for two electrons possessing parallel spins, the total spin quantum number, S=1/2+1/2=1. The spin multiplicity gives the number of states expected in the presence of an applied magnetic field and is determined by 2S+1.

A singlet state is the electronic state of a molecule, whose electrons with opposite spins are paired. Hence, in this case, S=0 and the spin multiplicity (2S+1) is 1. On the other hand, a triplet state has S=1 and a spin multiplicity of 3. In this case the electrons have the same spin, both 'spin-up' or both 'spin-down'. In the diagram above, E_0 corresponds to the singlet ground state. An electron can be raised to an excited state (E_3) in the presence of a photon of light. Assuming the energy gap between E_3 and E_2 is small, the electron decays non-radiatively, with phonon emission, to the lower state. Radiative decay will result from a transition from energy levels, E_2 or E_1 to the ground state E_0. If the excited state is a singlet state (say E_2), then the radiation emitted from this transition to singlet ground state is called fluorescence. These transitions are quantum mechanically allowed with a high transition probability. When a transition occurs between states of differing multiplicity, for example, a triplet to a singlet, say E_1 to E_0, the process is known as phosphorescence, and is quantum mechanically forbidden, with low transition probability [2].

3.2.1: Fluorescence Lifetime

The fluorescence lifetime or decay time (τ) is the average period of time a fluorescent molecule spends in an excited state prior to its return to ground state. The observed lifetime depends on both the radiative and non-radiative decay rates as given by equation 3.1,

$$K_{obs} = \frac{1}{\tau_{obs}} = \frac{1}{\tau_{rad}} + \frac{1}{\tau_{non-rad}} \qquad (3.1)$$

Where, $1/\tau$ is equal to the decay rate, κ, and where obs, rad and non-rad, refer to the observed, radiative and non-radiative lifetimes respectively.

The fluorescent complex of interest in this work has a triplet excited state and a singlet ground state, which results in a partially allowed transition of relatively long fluorescence lifetime τ. This is discussed further in the next section.

3.3: Ruthenium Complexes

The use of fluorescent transition metal complexes in the development of fluorescent optical sensing devices has become increasingly widespread due to the number of desirable characteristics they possess [3, 4]. Firstly, these compounds tend to be thermally, chemically, and photochemically stable, resulting in the increased long-term stability and durability of the sensors. They exhibit strong absorption in the blue-green region of the spectrum ensuring compatibility with a large range of suitable excitation light sources. The Stokes shift is the difference in wavelength between absorption and fluorescence maxima and for transition metal complexes this is relatively large, enabling the use of suitable filters to differentiate between excitation and emission light. Generally, these compounds have high quantum yields (ratio of number of photons emitted to those absorbed) and long lifetimes.

The dye complex used for sensor fabrication throughout this work was $[Ru(Ph_2phen)_3]^{2+}$ or Ru(II) tris(4, 7-diphenyl-1, 10-phenanthroline). The chemical structure of this compound consists of the ligand (Ph_2phen) attached to the Ru molecules via nitrogen atoms (N). Each Ru molecule is surrounded by three of these ligands.

The ruthenium complex has partially filled d orbitals, the ordering and occupancy of which determines the emissive properties [5]. The octahedral field of the ligand splits the five degenerate orbitals resulting in a triply degenerate t_{2g} level and a doubly degenerate e_g level. The magnitude of the energy difference is the crystal field splitting, Δ. An orbital diagram representative of this complex is shown in figure 3.2.

Figure 3.2: Simplified orbital diagram for Ru(II) tris(4, 7-diphenyl-1, 10-phenanthroline).

The ligands have both π and σ orbitals. However, only the π orbitals are significant for visible and near UV absorption and emission. There are π bonding (π) and π antibonding (π^*) levels, but only the π bonding levels are filled. Since the complex is low spin and all electrons are paired, the ground state is a singlet electronic state. The excitation of the complex results in the elevation of an electron to one of three possible excited states, namely,

(1.) The promotion of a d electron to another d level or a d-d transition.

(2.) The promotion of an electron from a π bonding orbital to a π^* antibonding orbital, is called a π-π^* state.

(3.) (a.) The promotion of a d electron to a π^* antibonding orbital is known as a MLCT or metal to ligand charge transfer state.

(b.) The promotion of an electron in a π bonding orbital to an unfilled d orbital is known as a LMCT or ligand to metal charge transfer state.

The metal to ligand charge transfer transition is the lowest in energy with respect to all other possible excited state transitions. Consequently, this state is primarily responsible for the absorption and emission characteristics of the complex. The long lifetime of these states result in the high susceptibility to oxygen quenching as discussed in the next section.

The $[Ru(Ph_2phen)_3]^{2+}$ has an absorption maximum at 450nm and the Stokes-shifted emission of the MLCT excited state to the ground state results in a fluorescence maximum at 608nm in aqueous solution and 611nm in sol-gel films.

It must be noted that there are many other ruthenium complexes, but the $[Ru(Ph_2phen)_3]^{2+}$ is deemed the most suitable for use to sense for dissolved oxygen for a number of reasons. Firstly, it is less susceptible to its environment than other complexes and is easily incorporated into the chosen sol-gel matrix. Also as previously mentioned it has a longer lifetime than any other ruthenium complex.

3.4: Fluorescence Quenching by Oxygen

Fluorescence quenching results in the decrease of fluorescence intensity of a given substance and generally can take the form of either static or dynamic quenching [2]. Static quenching occurs as a result of the formation of a non-fluorescent ground state complex between the fluorophore and the quencher. When this complex absorbs light it immediately returns to the ground state without the emission of a photon. In this work, the fluorescence quenching was solely due to dynamic quenching and hence there were no contributions from static quenching. Also, the quencher in question was oxygen.

The dynamic or collisional quenching results from collisional encounters between the fluorophore and the oxygen. In this case, the oxygen must reach the fluorophore within the lifetime of the excited state. Upon contact, the fluorophore returns to the ground state without the emission of a photon. Collisional quenching of fluorescence is defined by the Stern-Volmer equation [6]:

$$\frac{I_0}{I} = 1 + \kappa\tau_0[Q] = 1 + K_{SV}[Q] \qquad (3.2)$$

$$\frac{\tau_0}{\tau} = 1 + \kappa\tau_0[Q] = 1 + K_{SV}[Q] \qquad (3.3)$$

Where, I_o and I are the fluorescent intensities in the absence and presence of quencher (oxygen) respectively, [Q] is the quencher concentration, τ_0 and τ are the lifetimes of the fluorophore in the absence and presence of quencher respectively, and K_{SV} is the Stern-Volmer constant which is given by,

$$K_{SV} = \kappa\tau_0 \tag{3.4}$$

Where κ is the bimolecular quenching constant, which in turn is defined by,

$$\kappa \propto \alpha D \tag{3.5}$$

Where α is the oxygen solubility in the matrix and D is the diffusion coefficient of oxygen in the sensing film.

The result of the quenching process is a decrease in both the fluorescence intensity (I) and lifetime (τ) with increasing oxygen concentration. The sensor can be based on monitoring either the intensity or the lifetime. In this work, the sensor was intensity-based.

The Stern-Volmer constant (K_{SV}) is a measure of the degree of quenching. This in turn is proportional to the decay time, τ_0, hence the importance of choosing an oxygen sensitive dye with a long lifetime. Note also from equations 3.4 and 3.5 that the quenching is also related to the oxygen diffusion coefficient D in the film, hence the importance of film porosity.

In this work the quenching data is presented as a plot of I_0/I versus quencher concentration, [Q], which theoretically should yield a straight line with an axial intercept of 1 on the y-axis and a slope of K_{SV}, as discussed in the next chapter. The magnitude of K_{SV} for a particular sensing film is deemed a measure of the oxygen sensitivity of that film.

3.5: Summary

The basic operation of the dissolved oxygen sensor developed in this work was introduced in this chapter. The principles of fluorescence and collisional quenching and their importance in this work were documented. The choice of transition metal complexes, in particular, the use of $[Ru(Ph_2phen)_3]^{2+}$ was justified with details of its properties provided.

References

[1.] A. Gilbert, J. Baggot; Essentials **of Molecular Photochemistry**, 1991, Blackwell Scientific Publications, Oxford, Chapter 1

[2.] J. R. Lakowicz; Principles **of Fluorescence Spectroscopy**, 1983, Plenum Press, New York

[3.] J. N. Demas, B. A. DeGraff; Design **and Applications of Highly Luminescent Transition Metal Complexes**, *Anal. Chem.*, 1991, Vol. 63, No. 17, pp. 829

[4.] B. D. MacCraith, G. O'Keeffe, A. K. McEvoy, C. M. McDonagh; Development **of a LED based fibre optic sensor using sol-gel derived coatings**, *Proc. SPIE* 1994, Vol. 2293, pp. 110

[5.] O. Stern, M. Volmer; Z. *Physic*, 1919, Vol. 20, pp.183

[6.] A. K. McEvoy, **Development of an Optical Sol-Gel-Based Dissolved Oxygen Sensor**, PhD Thesis, 1996, Dublin City University (unpublished)

Chapter 4: Fabrication, Characterisation and Optimisation of Sensing Films

4.1: Introduction

The primary function of the dissolved oxygen sensor developed in this work is to monitor any changes in fluorescence intensity of the fluorophore, corresponding to changes in oxygen levels in the sensor environment. To successfully accomplish this, the sensing system must comprise some basic elements, namely, a suitable excitation source, fluorescent sample, filters, and a photodetector. This chapter details the laboratory-based sensing system developed. The steps involved in the production of the dye-doped sol-gel thin films are documented. Also, the sensitivity of these films, in terms of their oxygen detection capabilities is investigated.

4.2: Sensor Fabrication

Sensor fabrication involves the encapsulation of a fluorophore in a porous sol-gel thin film matrix. The first step in this process was to weigh the required amount of ruthenium complex (40,000ppm of dye by weight of silicon atom) into a clean glass vial containing a magnetic bob. Ethanol was then added to the vial to dissolve the dye. Water with a pH equal to 1 was prepared by adding some HCl to de-ionised water. Note it has previously been established that a pH of 1 provides the optimum catalysis conditions for the sensor films [1]. This pH1 water was then measured into the vial and the solution stirred for approximately ten minutes. The chosen precursor was added dropwise to the vial while stirring, to promote homogeneity. A lid was placed loosely on the vial and the sol was left to stir for 1 hour. After mixing, the sensing films were prepared by dipping the pre-prepared glass substrates into the sol as discussed previously. The films were then left to dry in the oven at 70°C for 18 hours.

For the purposes of this work the organically modified precursors methyltriethoxysilane (MTEOS) and ethyltriethoxysilane (ETEOS) were used. The films were fabricated with R values (water precursor ratios) equal to 2 or 4.

4.3: Instrumentation for Characterisation of Sensing Films

To enable the selection of the optimum film for dissolved oxygen sensing, each film must be tested in terms of its oxygen detection capabilities. This entailed exposing the films to water containing various amounts of dissolved oxygen and measuring the response of the films. A laboratory-based sensing system was developed previously for this purpose [1]. This system can be used in the detection of either gas-phase or aqueous phase oxygen. However, the application for the sensor in this project is to detect dissolved oxygen. The operation of this sensor is detailed in full in the following section.

4.3.1: Laboratory-based Characterisation System

The laboratory-based characterisation system comprises the basic elements previously mentioned, namely, an excitation source, fluorescent film, filters and a photodetector. A schematic of the system is shown in figure 4.1. A bright blue LED with spectral output centered at 470nm serves as the excitation source. Figure 4.2 shows that good overlap exists between this excitation output and the absorption spectrum of the ruthenium complex. The excitation light passes through a wide-bandpass filter, (400-505nm, Infrared Engineering, Maldon, Essex, UK) and is focused onto the sample by a lens. The fluorescent sample is held rigid at an angle of 45^0 to the LED beam inside a watertight cell. The fluorescence from the sample passes through a long-wave pass filter ($\lambda_{cut\text{-}on}$ =570nm, CVI Laser Corporation, Albuquerque, N.M., USA) and is focused by a lens onto the photodiode (Hamamatsu, S1223-01). It is important to note that this choice of filters minimises the amount of excitation light reaching the photodiode while enabling the full capture of the fluorescence signal. The LED is pulse modulated ($f_m \approx 1$kHz) enabling the use of a lock-in detection system, which assists in the discrimination against ambient light levels [2].

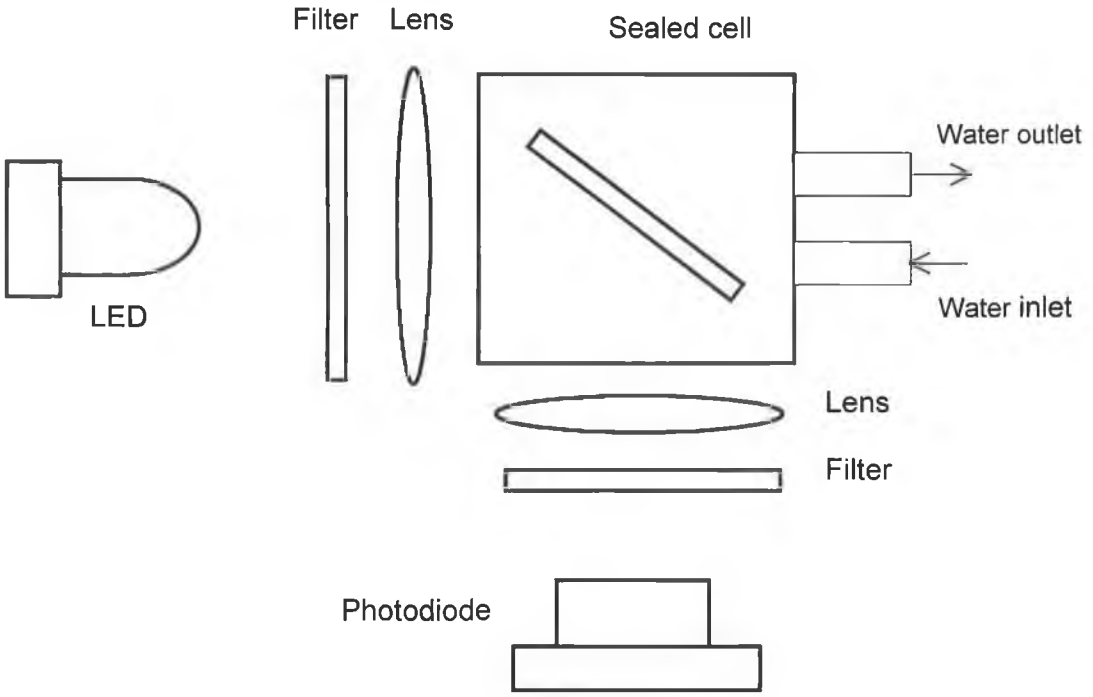

Figure 4.1: Schematic diagram of laboratory based characterisation system

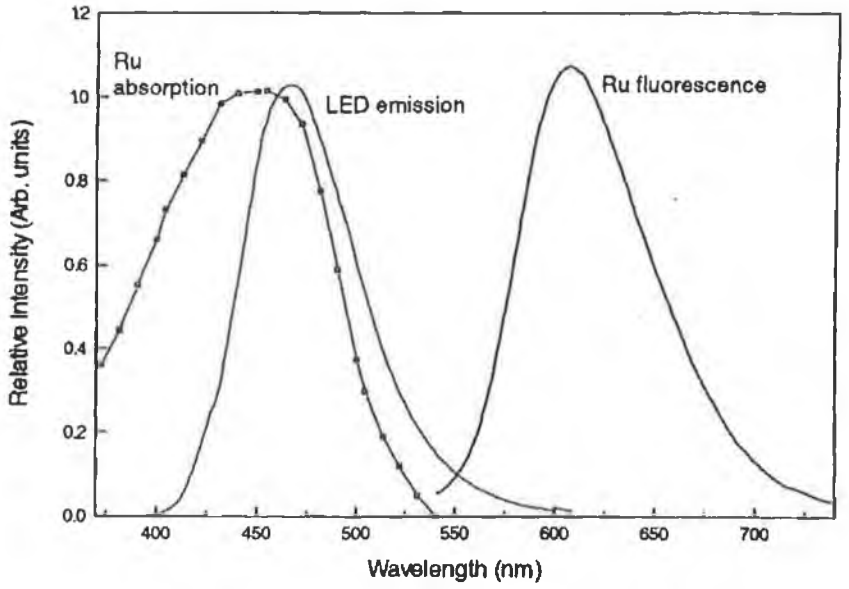

Figure 4.2: Overlap of LED spectral output and absorption of ruthenium complex

4.3.2: System for Obtaining Calibrated Dissolved Oxygen Solutions

Calibrated dissolved oxygen solutions were produced in the system shown in figure 4.3. The primary components are two gas cylinders containing oxygen and nitrogen, two mass flow controllers, a water reservoir and a magnetic stirrer. The mass flow controllers can accurately control the flow of gas from the two cylinders, enabling the ratio of the two gases to be altered depending upon the concentration of dissolved oxygen required. The gases are directed into the sealed reservoir of deionised water containing a magnetic bob and situated on a magnetic stirrer. The solution is stirred vigorously to facilitate the equilibration of the solution. These calibrated solutions are then flowed through a narrow bore tubing via a peristaltic pump to the characterisation cell containing the doped sol-gel-coated sensing film for measurement purposes.

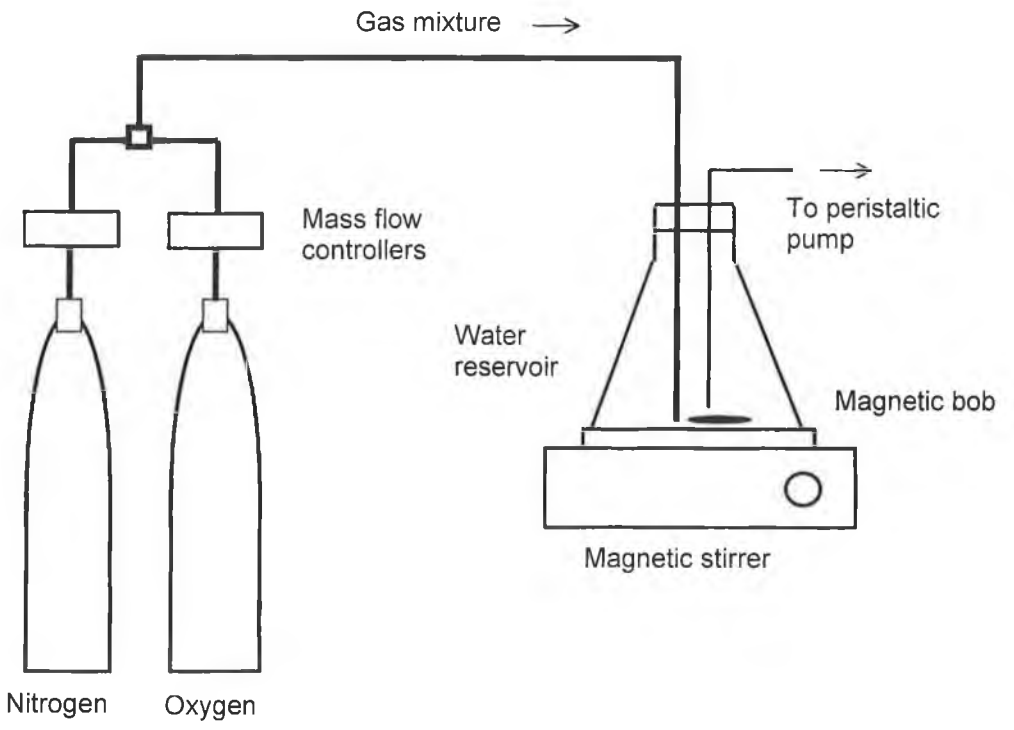

Figure 4.3: Schematic of system used to obtain calibrated dissolved oxygen solutions.

4.4: Measurement of the Quenching Response of Sensing Films

Referring back to section 3.4, the quenching response of a film may be determined by measuring the intensity, I, as a function of oxygen concentration, $[O_2]$, and plotting the Stern-Volmer relationship. The slope K_{SV} of this Stern-Volmer plot is proportional to the oxygen sensitivity of the particular film, and ultimately can be used to calibrate the dissolved oxygen sensor.

Prior to measuring the quenching response of a particular film, the baseline level must be determined. This involves placing a clean uncoated glass slide into the cell and flowing deionised water through the system. Thus, the background light levels can be measured and zeroed.

The quenching characteristics of the sensing film are measured by flowing a range of solutions ranging from 0 to 100% oxygenated water through the sample cell containing the sensing film. The sensor response to each environment is recorded. This data is then used to plot the corresponding Stern-Volmer graph as given by equation 3.2, from which K_{SV} may be calculated. An alternative method used in this study to characterise the quenching response of a particular film is to measure the intensity response to fully oxygenated water (100%) and fully deoxgyenated water (0%). From this data, a second parameter used to evaluate a sensing film is calculated. This parameter is the quenching response and is defined as:

$$Q_{DO} = \frac{I_{deoxy} - I_{oxy}}{I_{deoxy}} \qquad (4.1)$$

Where, I_{deoxy} is the fluorescence intensity in the presence of fully deoxygenated water and I_{oxy} is the fluorescence intensity in the presence of fully oxygenated water.

While K_{SV} is a measure of oxygen sensitivity over the full range of oxygen concentration, Q_{DO} is a more convenient indication of sensitivity based on the two extreme points of the oxygen calibration curve. Referring to equation 3.2,

$$Q_{DO} = 1 - \frac{I}{I_0} \qquad (4.2)$$

4.5: Optimum Sensing Films

Much work has been carried out previously to establish the optimal sensing films for dissolved oxygen sensing [3,4]. Typically, films fabricated with the precursor TEOS were found to have a quenching response Q_{DO} of approximately 23% [5]. However, films fabricated with the organically modified precursors MTEOS and ETEOS consistently yield higher quenching responses, as was verified during the course of this work. Figure 4.4 (a) and (b) show the quenching response of a R=2 MTEOS and R=2 ETEOS film respectively.

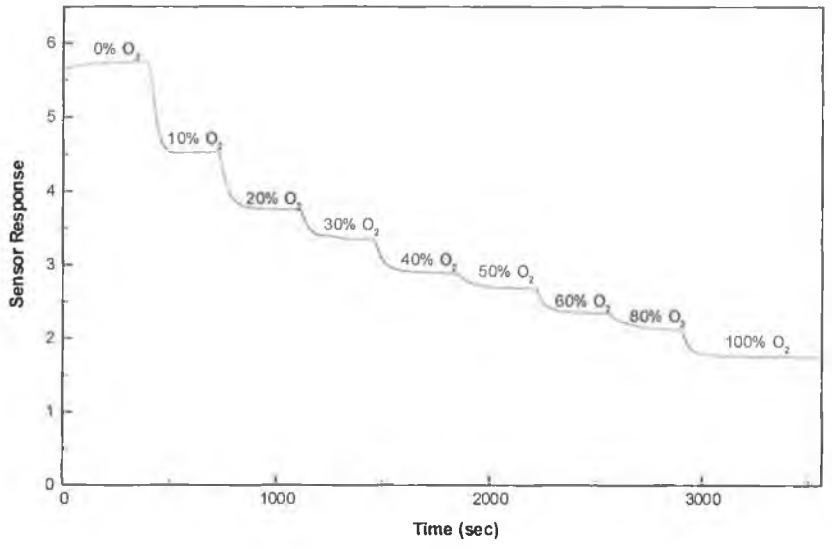

Figure 4.4 (a): Response of R=2 MTEOS film.

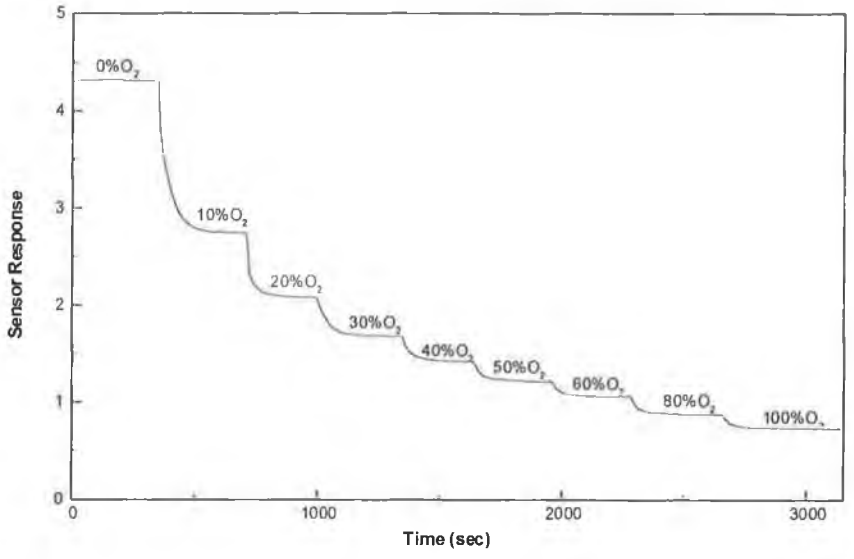

Figure 4.4 (b): Response of R=2 ETEOS film.

The Stern-Volmer plots corresponding to the calibration curves above are shown in figure 4.5. The Stern-Volmer constants (K_{SV}) may be deduced from the slopes of these plots. In the case of the R=2 MTEOS film the K_{SV} was calculated to be 0.0548ppm^{-1} and in the case of the R=2 ETEOS film the K_{SV} was calculated to be 0.1211ppm^{-1}. Note here that 100% oxygen in water corresponds to 40ppm.

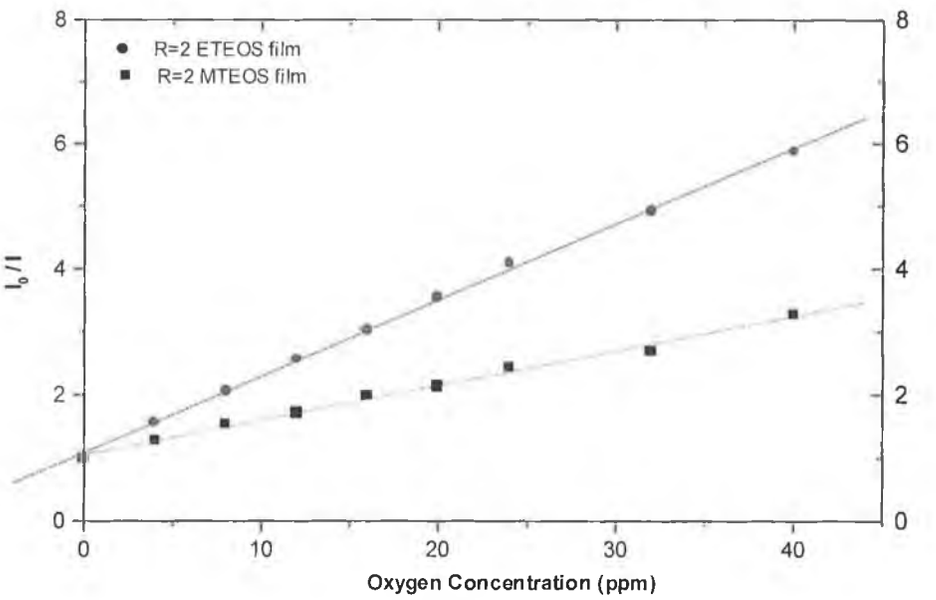

Figure 4.5: Stern-Volmer plots for R=2 MTEOS and R=2 ETEOS films.

These K_{SV} values correspond to Q_{DO} values of 70% and 83% respectively, far greater than that of the TEOS films. This is largely due to the surface polarity of the films. TEOS based films are known to have a large surface coverage of hydroxyl (OH^-) groups, thus rendering the films hydrophilic [6,7]. On the other hand ormosil films show a reduction in the amount of surface hydroxyl groups due to the presence of surface alkyl groups [8]. In the case of MTEOS, the alkyl groups are methyl groups (CH_3) and for ETEOS the alkyl groups are ethyl groups (C_2H_5). Since these alkyl groups are hydrophobic in nature, their predominance in ormosil films results in an overall reduction in the sensing films' affinity for water [6].

It is proposed that the operation of the dissolved oxygen sensor in this work is based on the principle whereby the oxygen partitions out of the water at the film/water interface and accesses the ruthenium dye in gas phase. The hydrophobic nature of the ormosil films is clearly conducive to this partitioning effect. Hence by increasing the hydrophobicity of the sensing film an enhancement of the partitioning process is observed. Consequently, the sensing operation is more efficient and results in an increase in the recorded quenching response. Previous work carried out in this laboratory used contact angle measurements to determine the degree of hydrophobicity of various sol-gel films [6]. This work concluded that ETEOS films are more hydrophobic than MTEOS films, which was verified by the quenching results obtained in this work for the MTEOS and ETEOS films. Since ETEOS is more hydrophobic than MTEOS it is expected that the quenching response for ETEOS be higher than that obtained for MTEOS, as is the case above. Finally, it must be noted that this gas partitioning is not 100% efficient. There is also a relative contribution to the fluorescence quenching by the aqueous phase oxygen in the pores that is significant.

4.6: Summary

The development of a sensing system for laboratory testing has been documented. Both the instrumentation used, and the methods of sensing film fabrication have been detailed. The advantages of using hydrophobic films for the purposes of dissolved oxygen sensing were highlighted and the choice of MTEOS and ETEOS films as optimum films justified.

References

[1.] A. K. McEvoy, **Development of an Optical Sol-Gel-Based Dissolved Oxygen Sensor,** PhD Thesis, 1996, Dublin City University (unpublished).

[2.] P. C. Hauser, S. S. Tan, **All-solid state instrument for fluorescence-based fibre optic sensors,** *Analyst*, 1993, Vol. 118, pp. 991-995.

[3.] C. McDonagh, B. D. MacCraith, A. K. McEvoy, **Tailoring of sol-gel films for optical sensing of oxygen in gas and aqueous phase,** *Anal. Chem.,* 1998, Vol. 70, No. 1, pp. 45-50.

[4.] P. Lavin, C. M. McDonagh, B. D. MacCraith, **Optimisation of ormosil films for optical sensor applications,** accepted for publication in *J. Sol-Gel Sci. Technol.,* 1998.

[5.] C. M. McDonagh, A. M. Shields, A. K. McEvoy, B. D. MacCraith, J. F. Gouin, **Optical sol-gel-based dissolved oxygen sensor: progress towards a commercial instrument,** *J. Sol-Gel Sci. Technol.,* 1998, Vol. 13, pp. 207-211.

[6.] P. Lavin, **Optimisation of ormosil thin films for sensor applications,** MSc. Thesis, 1997, Dublin City University (unpublished).

[7.] K. Matsui, M. Tominaga, Y. Arai, H. Satoh, M. Kyoto, **Fluorescence of pyrene in sol-gel silica derived from triethoxysilane,** *J. Non-Cryst. Solids,* 1994, Vol. 169, pp. 295-300.

[8.] P. Innocenzi, M. O. Abdirashid, M. Guglielmi, **Structure and properties of sol-gel coatings from methyltriethoxysilane and tetraethoxysilane,** *J. Sol-Gel Sci. Technol.,* 1994, Vol. 3, pp. 47-55.

Chapter 5: Long Term Stability of Sensing Films

5.1: Introduction

This chapter details a number of the studies carried out on the optimum sensing films, namely those fabricated with 100% MTEOS and 100% ETEOS. In particular, an investigation into the long-term stability of these films in both air and water was undertaken to establish if leaching or photobleaching of the entrapped dye was occurring, as is often the case in fluorescence based sensors. Additionally, the stability of the calibration curves of the sensing films was investigated.

5.2: Leaching Studies

Given the nature of the dissolved oxygen sensor, it is important to monitor film performance in flowing water over a relatively large period of time. It has been observed that some sol-gel coatings tend to release some of their incorporated dye when immersed in liquid [1,2,3]. This dye leaching is due to the fact that the dye complex is not chemically bound but merely physically entrapped within the sol-gel matrix. Consequently, a reduction of the fluorescence intensity occurs. This aspect of the sensor performance is clearly undesirable, so a number of experiments were carried out to try to minimise the leaching effect.

In order to monitor the long-term stability of the sensing films their response in flowing water was monitored continuously for a period of approximately three days. These experiments were carried out using the system shown over in figure 5.1.

The coated slide to be monitored was mounted in the characterisation cell under blue LED illumination and aerated water was flowed continuously through the closed system via the peristaltic pump. The output from the photodiode was connected to a data logger, which enabled the sensor response to be sampled over the required period.

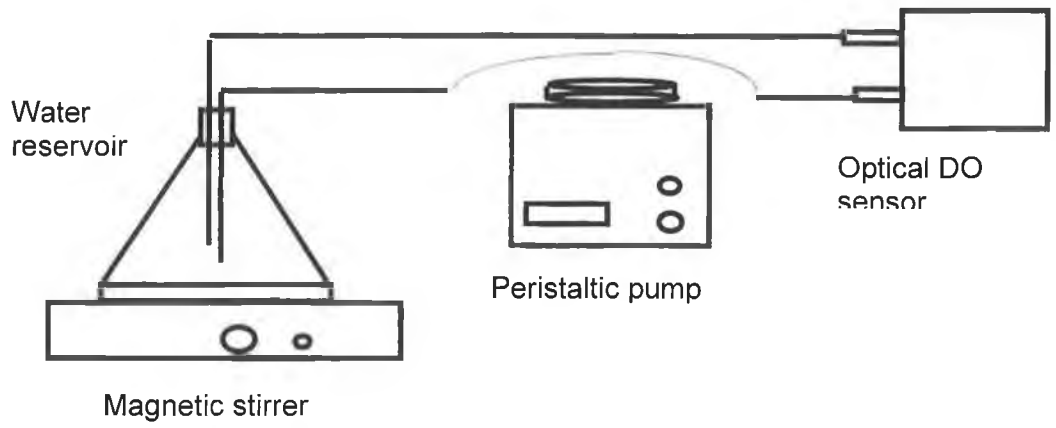

Figure 5.1: Long term stability system.

Previously, the optimum films for the purposes of dissolved oxygen sensing, were identified as those fabricated with 100% MTEOS and 100% ETEOS [4.] as discussed in chapter 4. Initially the long-term stability study involved testing these optimum films. The immersion of each of these films in flowing water over a period of time resulted in a significant reduction in the output signal from the sensor, with decreases of 12% and 18% respectively, recorded. Figure 5.2 compares the response of both the MTEOS and ETEOS films. It must be noted that that the response of the photodetector, the LED output, and the filter transmission were tested and found to be stable over time.

Clearly the ETEOS film exhibited greater leaching effects than the MTEOS film. It is thought that the smaller pore size in the MTEOS films results in better dye entrapment and hence less leaching. The ETEOS films on the other hand have a more open structure, with larger pore sizes, the result being greater leaching effects. This more open structure of ETEOS films compared to those fabricated with MTEOS can be correlated to the larger ethyl groups.

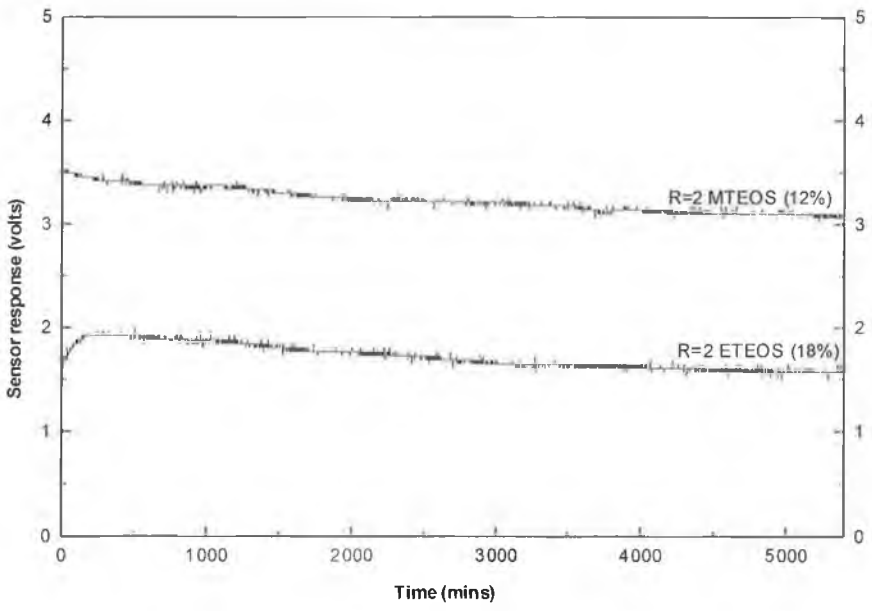

Figure 5.2: Stability of MTEOS and ETEOS films in flowing water.

In order to minimise the leaching problem the dopant must be encapsulated in a tightly closed cage. It is apparent from the above results that the pore size of the R=2 sol-gel films is too large. However, as was previously discussed in chapter 2, increasing the R value (water precursor ratio) during fabrication of the sol, results in the production of films with smaller average pore size and hence, better dye entrapment. It is predicted that the overall result of this is a film which exhibits less leaching than that of either the R=2 films. The response of a R=4 MTEOS film in flowing water was investigated and the result is compared with that of the R=2 MTEOS film and shown in figure 5.3.

The signal reduction recorded for the R=4 film was only 1%, much less than that obtained for the R=2 MTEOS film. In fact the 1% reduction for the MTEOS film can be regarded as being within measurement error. It is expected that an error of at least 1% is present due to temperature effects (see chapter 8). Hence it is concluded that little or no leaching occurs in R=4 MTEOS films. The smaller average pore size achieved by increasing the R value results in better entrapment of the dye complex, which in turn minimises the observed leaching.

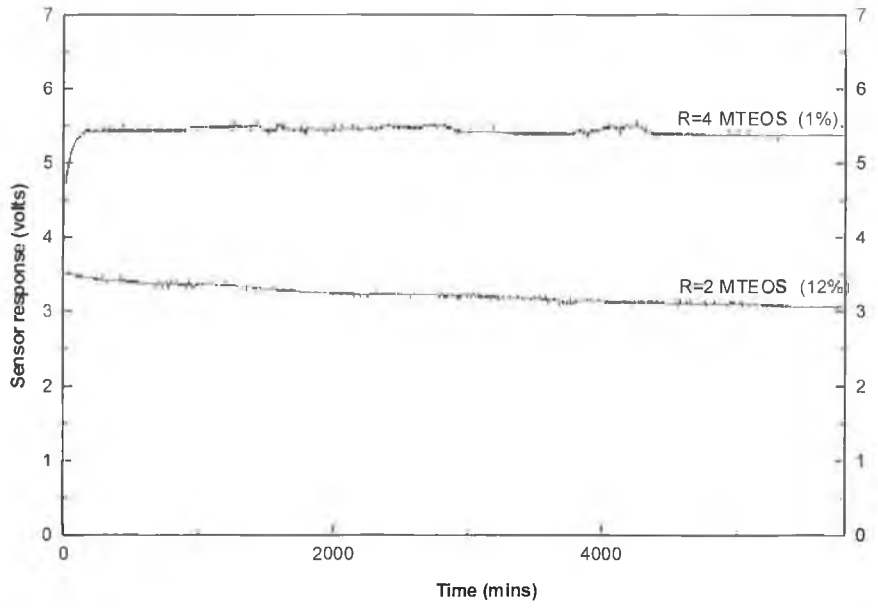

Figure 5.3: Stability of R=2 and R=4 MTEOS films in flowing water.

It must be noted that the increase in response at the beginning of both the R=2 ETEOS and R=4 MTEOS traces were correlated to ambient temperature changes caused by the idiosyncrasies of the air conditioning system in the laboratory. Further studies regarding the temperature dependence of the sensor response are provided in chapter 8.

5.2.1: Barrier Layer

As discussed in the next chapter and in chapter 7, this project involved the development of a prototype dissolved oxygen sensor for testing in the field. With the production of a dip probe version of the prototype, a problem was encountered, since the fluorescence detector was no longer enclosed in a light tight housing but was now exposed to ambient light. The need for optical isolation prompted the use of a black silicone rubber layer for this purpose. However, it was thought that this rubber coating might have another use, namely to act as a barrier layer that would prevent or minimise leaching. While the use of the rubber coatings for optical isolation is discussed further in chapter 7, some details regarding the effect of the rubber coating on leaching are provided in this chapter.

An experiment was carried out to test the effectiveness of coating the sensing film with an oxygen permeable layer, which would prevent the surrounding water from flushing out the incorporated dye. Both the R=2 and the R=4 MTEOS films were chosen for this purpose. The R=2 MTEOS film was coated with a 50% w/v solution of silicone rubber (Dow Corning 3140 RTV) in xylene. The R=4 MTEOS film was coated with a 62% w/w solution of silicone rubber (Wacker N189) in toluene.

Further details regarding the choice of silicone rubbers and the coating process will be provided in the chapter 7, since the primary purpose of the barrier layer was for optical isolation. Once again the response of the films in flowing water was monitored and the results are shown in figure 5.4

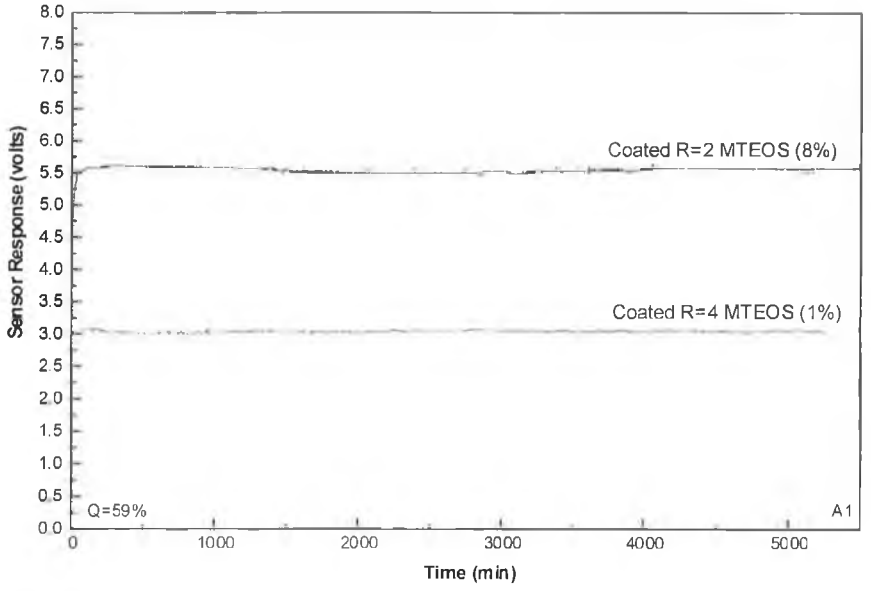

Figure 5.4: Stability of R=2 and R=4 MTEOS films coated with silicone rubber.

The signal reduction for the coated R=2 film was 8%, a decrease on that recorded for the uncoated film shown in figure 5.3. For the coated R=4 film the signal reduction was 1%, the same as that measured for the uncoated film, which is within the experimental error.

The R=2 MTEOS and ETEOS films were previously identified in chapter 4 as the optimum films for use as dissolved oxygen sensors due to their high quenching responses of 70% and 83% respectively. However it is apparent from this study that they are particularly susceptible to leaching problems even when coated with a barrier layer. The criteria for practical dissolved oxygen sensors dictates that they be resistant to such leaching problems, particularly for applications, which require continuous monitoring.

R=4 MTEOS films have a lower oxygen sensitivity to either the R=2 MTEOS or R=2ETEOS films, with a quenching response of 60%. Despite this, they are a more attractive prospect for use in dissolved oxygen monitoring, since they exhibit no leaching effects. In fact it must be noted that the signal to noise ratio for this system is such that the loss of sensitivity in going from R=2 to R=4 can be tolerated in order to improve the sensor stability.

A summary of the leaching study results is provided in table 5.1 below.

FILM:		**Signal Reduction: (%) ± 2%**
R=2 ETEOS		18
R=2 MTEOS		12
R=4 MTEOS		1
Coated with silicone rubber	R=2 MTEOS	8
	R=4 MTEOS	1

Table 5.1: Results of leaching study.

5.3: Photobleaching Studies

The photostability of the ruthenium dye is an important consideration for the dissolved oxygen sensor developed in this project, given that the direct measurement of the fluorescence intensity determines the sensor output. It has been reported elsewhere that continuous excitation by a blue LED, such as that used in this case, results in photobleaching of the dye when immobilised in polymer matrices [5]. Specifically, a photon of light causes an irreversible change in the electronic structure of the fluorescent molecule whereby the molecule no longer fluoresces. This means an irreversible decrease in the fluorescence intensity occurs with time. This effect is frequently observed but not greatly understood by those working in this area. The photobleaching effect increases as the intensity of the light source increases and in the case of oxygen sensitive ruthenium complexes, is enhanced in the presence of oxygen.

A recent conference report on the photobleaching of a range of ruthenium complexes indicated that the oxygen quenching efficiency is affected as a result [6]. The study also reported concentration dependent effects. Hence, in order to investigate this effect in doped sol-gel films, the response of two MTEOS films in air was recorded continuously for approximately two days using the data logger. The results obtained are shown in figure 5.5.

Clearly no photobleaching of the dye complex is occurring for the particular LED power maintained throughout this project. Note the origin of the random fluctuations in intensity in figure 5.5 is due to temperature fluctuations. The long-term stability experiments were not carried out under constant temperature conditions.

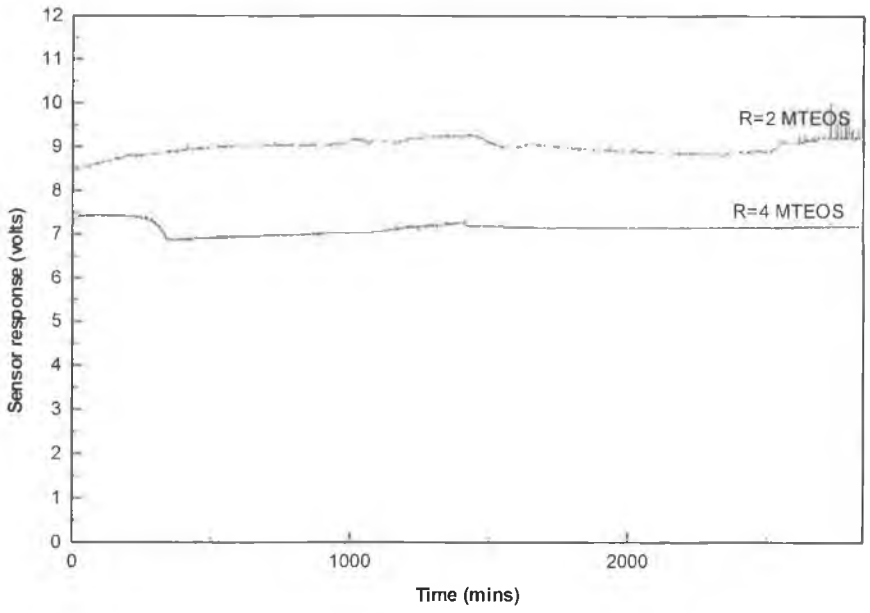

Figure 5.5: Stability of MTEOS films in air.

5.4: Stability of Calibration Curves

One of the primary goals of this project is the development of a commercially viable dissolved oxygen sensor. Such a sensor requires a comprehensive calibration protocol, which incorporates among other things effective temperature compensation. The calibration curve of the sensing film is required for this protocol since it provides the relationship between the measured fluorescence intensity and the required oxygen concentration. However, before such a protocol could be developed it is essential to establish the stability of the calibration curve, to determine if any changes occur over a period of time.

An investigation was carried out over a period of approximately ten months to establish the stability of the calibration curves for individual films. The study involved exposing the sensing film to a calibrated solution of oxygenated water and recording the resulting fluorescence intensity. This was repeated for various concentrations of dissolved oxygen in the water and the associated calibration curve was plotted in the form of a Stern-Volmer plot.

It is to be expected that the intensity value for any particular oxygen concentration will change from scan to scan due to slight variations in the position of the slide and temperature effects. Hence the ratio I_0/I was calculated for each particular oxygen concentration. This parameter is the ratio of the fluorescence intensity in the absence of oxygen (I_0) to that for a particular oxygen concentration (I). It provides the means for determining the step-sizes within the calibration curve and so should remain constant for the oxygen concentration in question. This data is expressed in terms of the Stern-Volmer relationship defined previously, the slope of which, K_{SV}, is related to the degree of quenching in the film. The parameter, Q_{DO}, as defined in equation 4.1 was also used to characterise the stability of a particular film.

Over a period of ten months the stability of calibration, of a R=2 MTEOS and a R=2 ETEOS film was monitored and a selection of the Stern-Volmer plots are shown in figures 5.6 and 5.7.

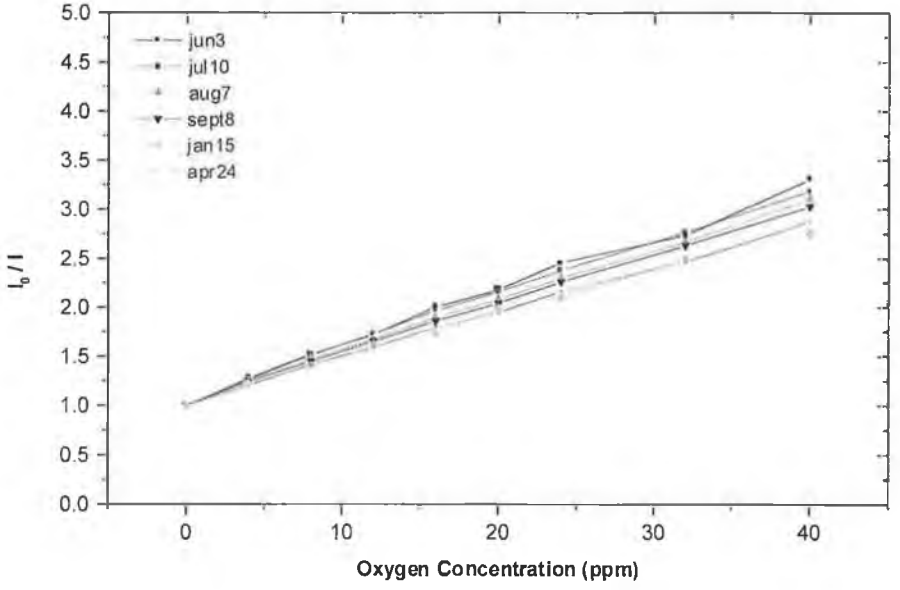

Figure 5.6: Stern-Volmer plots for R=2 MTEOS film in aqueous phase.

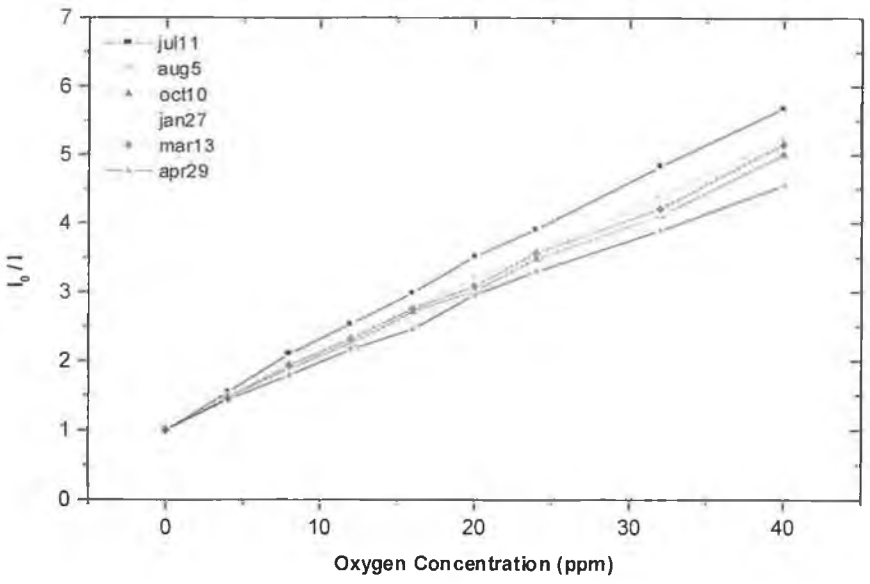

Figure 5.7: Stern-Volmer plots for R=2 ETEOS film in aqueous phase.

It is apparent in both cases that the more recent data has a lower Stern-Volmer slope than that of the earlier data. The slope values (K_{SV}), corresponding to the data in the above graphs are presented in tables 5.2 and 5.3. From these figures it was calculated that the K_{SV} has decreased by 17% in the case of the MTEOS film and by 23% for the ETEOS film, over the course of the ten months. In terms of the quenching response, Q_{DO}, this decrease in sensitivity is approximately 6% and 4% for the MTEOS and ETEOS films respectively. Figure 5.8 shows the quenching response, Q_{DO}, plotted as a function of time.

Date:	K_{sv} (ppm^{-1}):
3/6/97	0.0558
10/7/97	0.0540
7/8/97	0.0517
8/9/97	0.0502
15/1/98	0.0443
24/4/98	0.0462

Table 5.2: Stern-Volmer constants corresponding to data in figure 5.6.

Date:	K_{sv} (ppm^{-1}):
11/7/97	0.116
5/8/97	0.105
10/10/97	0.0979
27/1/98	0.0942
13/3/98	0.102
29/4/98	0.0888

Table 5.3: Stern-Volmer constants corresponding to data in figure 5.7.

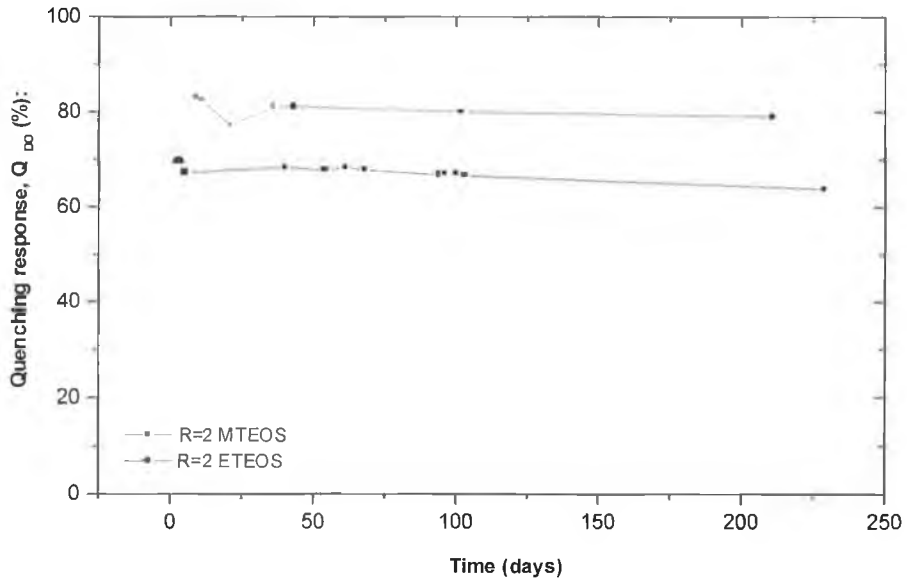

Figure 5.8: Quenching response, Q_{DO}, as a function of time for both MTEOS and ETEOS films.

Initially, during the investigation it was thought that the decrease in sensitivity of the two films was due to changing temperature. However, data recorded in the latter half of the study was correlated with ambient temperature in the laboratory, and it was concluded that the effect was not temperature related but rather, due to changes occurring in the film microstructure. Specifically, it seems likely that the film microstructures are undergoing a slow evolution resulting in a denser pore structure. It is thought that this is due to continuous slow hydrolysis and condensation reactions occurring in the films, possibly facilitated by the moisture surrounding the film.

Another possible reason for the decrease in sensitivity of the R=2 MTEOS and R=2 ETEOS films is leaching of the incorporated dye complex. Figure 5.2 clearly showed that leaching affects the performance of these films over the course of three days. Hence it is likely that some degree of leaching has occurred in both films in the stability of calibration study carried out over ten months. Another study was carried out in order to establish if R=4 MTEOS films are more stable than the R=2 films, since it was shown previously that the R=4 MTEOS films exhibit no leaching effects.

Hence, the study of two different R=4 MTEOS films, one coated with silicone rubber (62% w/w solution of Wacker N189 rubber in toluene), was carried out over the course of five weeks. Both films were stored in water in between experiments since this reflects the use of a commercial dissolved oxygen sensor, which sits in water for the periods of time between measurements. Once again the stability of calibration was monitored. The results obtained are shown in figures 5.9 and 5.10.

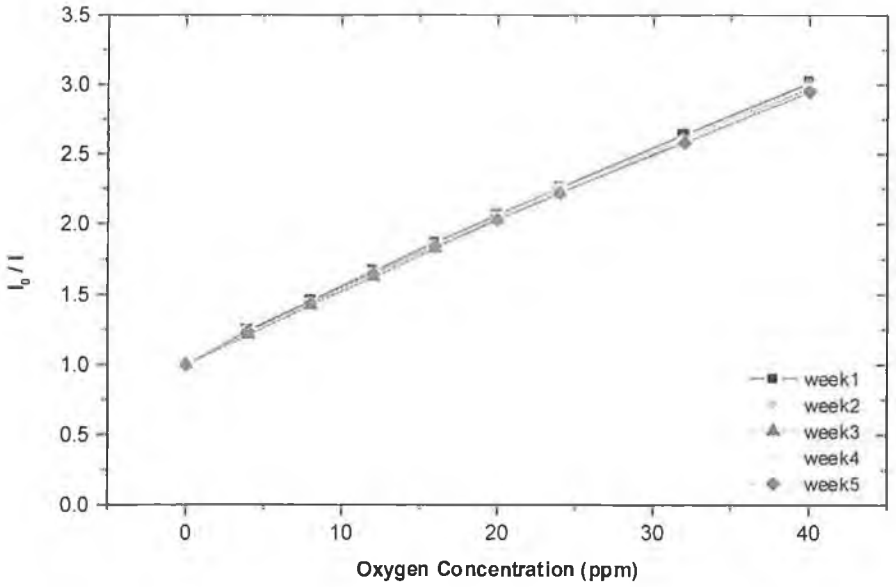

Figure 5.9: Stern-Volmer plots of R=4 MTEOS film stored in water.

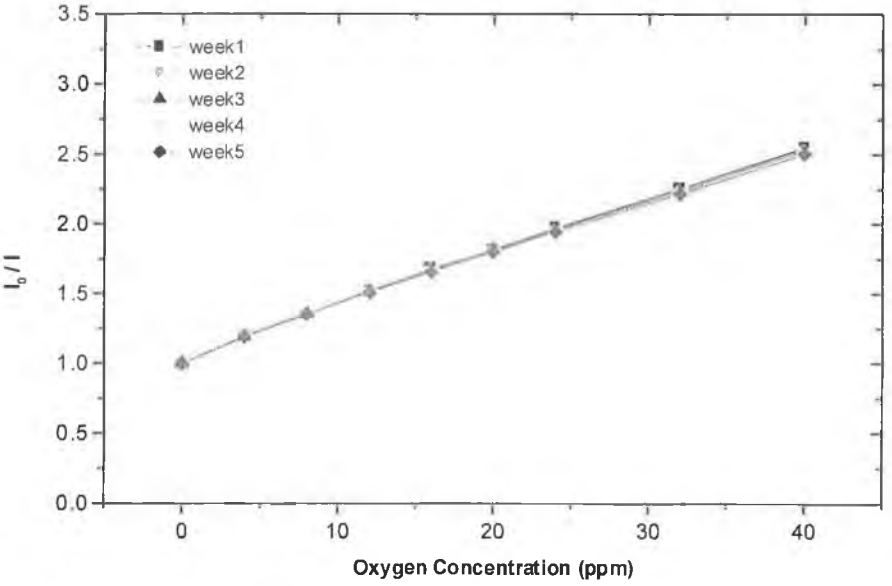

Figure 5.10: Stern-Volmer plots of rubber coated R=4 MTEOS film stored in water.

This data relating to figures 5.9 and 5.10 are tabulated below in tables 5.4 and 5.5. As before, both films exhibited a decrease in oxygen sensitivity, with a decrease in the Stern-Volmer constant of approximately 3% recorded in each case.

Date:	K_{sv} (ppm^{-1}):
Week 1	0.0500
Week 2	0.0495
Week 3	0.0494
Week 4	0.0491
Week 5	0.0483

Table 5.4: Stern-Volmer constants for R=4 MTEOS film.

Date:	K_{sv} (ppm^{-1}):
Week 1	0.0383
Week 2	0.0380
Week 3	0.0377
Week 4	0.0373
Week 5	0.0371

Table 5.5: Stern-Volmer constants for R=4 MTEOS film coated with silicone rubber.

The decrease in the Stern-Volmer constant is significantly lower for both the R=4 MTEOS films, although it must be noted that the latter study only took place over a five week period.

Given the reduction in sensitivity of both the R=4 MTEOS films it is unlikely that leaching is the cause of the problem but rather evolution of the sensing films microstructures to denser pore structures. These changes in the sensing film microstructures require further investigation since it is essential to produce a film structure that fully stabilises in a much shorter time. These investigations must be completed before any calibration protocol for the commercial sensor can be developed. Note that it is also clear from this work that the silicone rubber layer has no effect on the long-term stability of the calibration curves.

5.5: Summary

This chapter traced the investigation into the long-term stability of the sensing films. It was found that tailoring of the sol-gel film fabrication parameters could be used to minimise any leaching effects and the use of a barrier layer was also effective for this purpose. The stability of the calibration curves of various films was studied. The lack of stability of the films due to a changing microstructure highlighted the need for the production of a sensing film with a faster stabilisation time. It is concluded from the above that R=4 MTEOS films are the optimum films for use in the prototype sensor discussed in chapter 6.

References:

[1.] T. M. Butler; **Development of Evanescent Wave pH Sensors Based on Coated Optical Fibres,** 1996, PhD Thesis, Dublin City University, (unpublished).

[2.] P. Lacan, P. LeGall, J. Rigola, C. Lurin, D. Wettling, C. Guizard, L. Cot; **Sol-gel derived optical pH sensors,** Proc. SPIE, Vol. 1758, Sol-Gel Optics II, 1992, pp. 464-475.

[3.] S. C. Kraus, R. Czolk, J. Reichert, H. J. Acher; **Optimisation of the sol-gel process for the development of optochemical sensors,** *Sensors and Actuators B*, 1993, Vol. 15-16, pp. 199-202.

[4.] A. K. McEvoy, **Development of an Optical Sol-Gel-Based Dissolved Oxygen Sensor,** PhD Thesis, 1996, Dublin City University (unpublished).

[5.] J. N. Demas, B. A. DeGraff; **Design and applications of highly luminescent transition metal complexes**, *Anal. Chem.*, 1991, Vol. 63, pp. 829-837.

[6.] P. Hartmann, M. J. P. Leiner, P. Kohlbacker; **Photobleaching of Ruthenium complexes in polymers used for oxygen optodes and its inhibition by singlet oxygen quenchers,** Europt(r)ode IV, 1998, Munster, Germany, Oral presentation.

Chapter 6: Design of Prototype Dissolved Oxygen Sensor

6.1: Introduction

One of the objectives of this project is the development of a high performance dissolved oxygen sensor suitable for commercialisation. To date the laboratory-based system has proved very successful for sensing film development and optimisation, but the nature of commercial sensors dictates that the design be as compact, rugged, and cost-effective to produce, as possible. The laboratory-based systems all-solid state design indicates the potential to fulfil these pre-requisites, however it is apparent that a number of modifications to both the mechanical design and the electronics are required in order to achieve this. This chapter traces the evolution of the design of a prototype dissolved oxygen sensor and the characterisation of its performance initially in gas-phase, then in aqueous phase. The sensor was designed by the optical sensors team, Dublin City University and constructed by PEI Technologies, Dublin City University. In total, three versions of the prototype were implemented, and details regarding each of the three are presented in this chapter.

6.2: Design Considerations

One of the primary objectives of the prototype development was the implementation of a dip probe configuration, which could be immersed into a sample of water for testing. Obviously this had many implications for the design of the prototype, since the entire sensor would be dipped into the water. Most importantly, all elements of the sensor, namely, the optics and electronics must be encased in water tight housing with only the sensing films exposed to the water. Also as previously mentioned, the nature of the dissolved oxygen sensor dictates that it be as compact and portable as possible. Hence, in order to facilitate both these prerequisites, the physical design of the laboratory-based sensing system was completely altered.

Previously as shown in figure 4.1, all of the optics were outside the characterisation cell that housed the sensing film. Additionally, the electronics were housed in a separate box away from the sensor head. However in the case of the prototype, the electronics, optics and the sensing film were all encased in the sensor head, as shown in figure 6.1. The new optical layout consisted of the fluorescence photodiode positioned perpendicular to the sensing film in order to detect the fluorescence. On one side of this fluorescence photodiode, the blue LED was placed at a 45° angle to the film, and on the other side a LED monitoring photodiode was also placed at a 45° angle to the film.

With regard to the sensing films used, instead of the double-sided films used in the laboratory-based system, new sensing films were fabricated with the sol-gel coating on just one side of the glass substrate. This is due to the fact that the prototype system employs back illumination of the single-sided film whereby the LED excitation and photodiode detection of the fluorescence is through the uncoated side of the film. Water is only circulated around the coated side of the film allowing access by the dissolved oxygen to the entrapped ruthenium complex as before. Hence unlike the laboratory-based system the water is excluded from the light path.

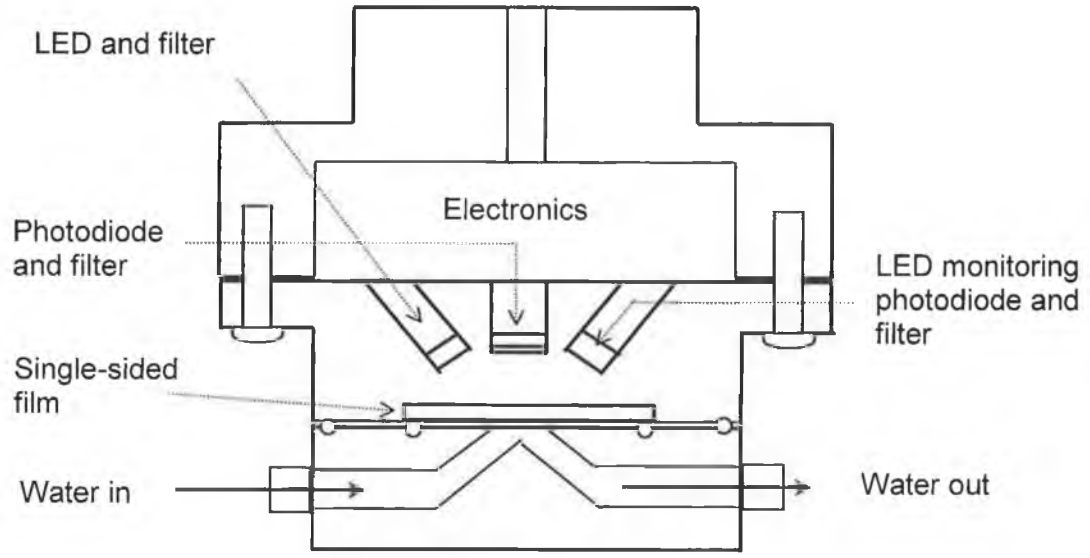

Figure 6.1: Schematic of prototype sensor head.

All the electronics were now encased in the sensor head as shown in figure 6.1. Schematics of the electronic circuits are provided in appendix 1. Both the LED driver and the photodiode detection circuitry were redesigned and built on two circular PCBs approximately 8cm in diameter and were housed above the optical elements of the sensor. This close proximity of the photodiode to the detection circuitry and their enclosure in light tight housing effectively eliminated any 50Hz noise pick-up from ambient light. It must be noted that during testing and characterisation of the system, one of these boards remained outside the sensor head to enable easy access for offsetting purposes.

The compact design of the sensor head introduced another consideration, namely the problem of too much LED light. As in the original laboratory-based system, the LED was initially driven by a pulsed current of 60-70mA, resulting in a lot of blue excitation light directed at the sensing film. A large portion of this light was reflected back from the film in the direction of the photodiode. Due to a certain transmission overlap between the wide band pass filter (located in front of the LED) and the long wave pass filter (located in front of the photodiode) this reflected blue light was measured by the photodiode via lock-in detection of the pulsed signal. Hence when a coated slide was placed in the cell, much difficulty was encountered trying to detect the small pulsed fluorescence signal, in particular, changes in this small signal against the constant background of the excitation light. To overcome this problem, the LED current was reduced considerably from pulsed 60-70mA to 10mA DC level and the system was tested.

Reducing the LED current effectively reduced the amount of light from the LED and so the background signal was reduced. The fluorescence signal and in particular the changes in this signal when going from a 100% oxygenated environment to a 100% nitrogenated environment were now clearly detectable. It was found that the LED current could be reduced to 2mA and still maintain successful operation. Obviously this low operating current will be an advantage when the sensor is battery powered since the lower currents imply a longer life for the batteries. This use of DC current to drive the LED has eliminated the need for a lock-in chip and phase sensitive detection and so has considerable implications for the final product, in particular the effect of ambient light on its successful operation, as discussed later in this chapter.

Finally, it must be repeated that the primary objective of the prototype design was the development of a probe that could be dipped into the water sample to be tested. This objective was achieved. However, for the purposes of characterisation of the performance of the instrument, a flow cell was designed. This attachment can be seen in figure 6.1.

6.3: Characterisation of Prototype Sensor – Version 1:

6.3.1: Gas-phase Results

Preliminary testing of the dissolved oxygen prototype was carried out by monitoring its response to oxygen gas. Figure 6.2 shows the response of a single-sided R=2 MTEOS film going from a 100% oxygen gas environment to a 100% nitrogen gas environment. For comparison purposes, a gas-phase scan was carried out on the same sensing film using the laboratory-based system. The results of this are shown in figure 6.3.

Looking at the two graphs it can be seen that the response times on the prototype system are slightly slower than those measured for the conventional system. This was thought to be due to the mechanical design of the flow cell, which was not allowing the oxygen direct access to all of the fluorescing sensing film. Hence the oxygen was taking longer to quench the fluorescence. However, the values recorded for the quenching response of the film were found to be consistent (78 +/- 2%) when repeated, and when compared to those obtained using the same film in the laboratory system. Overall the results were promising, although they highlighted the need for some changes, in particular to the design of the flow cell.

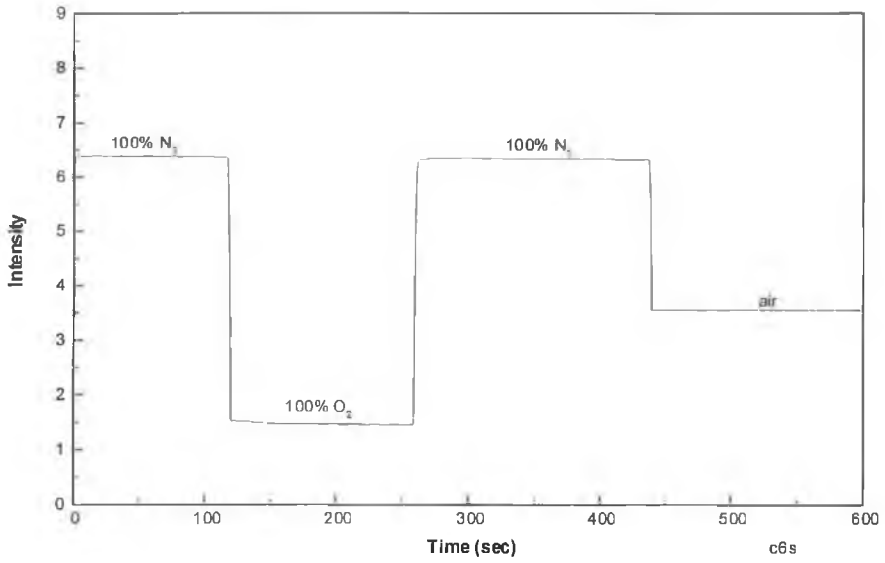

Figure 6.2: Response of single-sided R=2 MTEOS film in gas-phase using the prototype system.

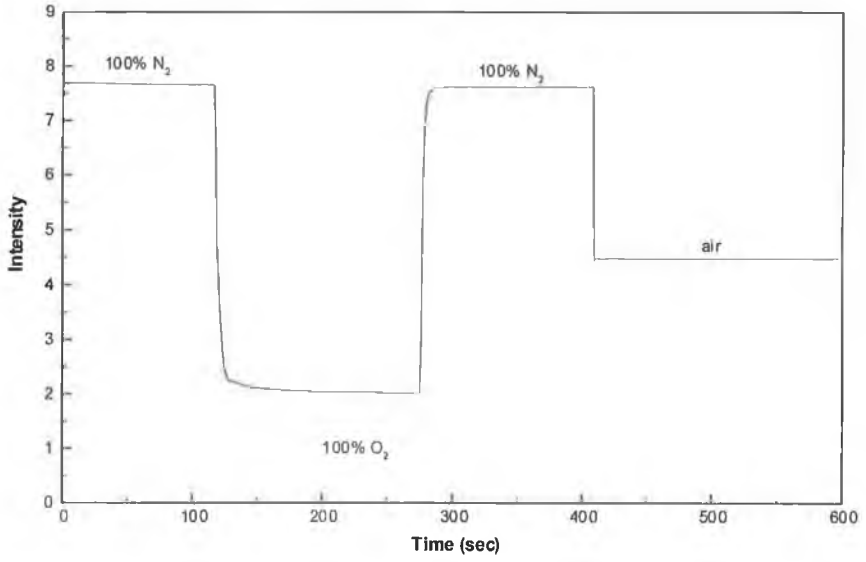

Figure 6.3: Response of single-sided R=2 MTEOS film in gas-phase using the laboratory-based system.

6.3.2: Aqueous-phase Results

After the initial gas-phase tests, the testing of the prototype was extended to the detection of dissolved oxygen. However the problem encountered in gas-phase testing was magnified in aqueous phase. A response time of greater than 25 minutes highlighted the inadequacy of the flow cell design and prompted the alteration of the shape of the flow cell. It seemed that much of the oxygenated/nitrogenated water solutions were flowing straight through the sensor head without actually fully accessing the film surface area. However, it was found that when the sensor head was turned upside down and tested, results were much improved. Figure 6.4 shows the response of a single-sided R=2 MTEOS film in aqueous phase.

The quenching response calculated for the R=2 MTEOS film was found to be approximately 60%. The results were found to be reproducible for the same film in aqueous phase when repeated. The corresponding response and recovery times were calculated and found to be approximately 15sec and 59sec respectively, which is very promising. However, the necessity to operate the sensor upside down is obviously unsatisfactory.

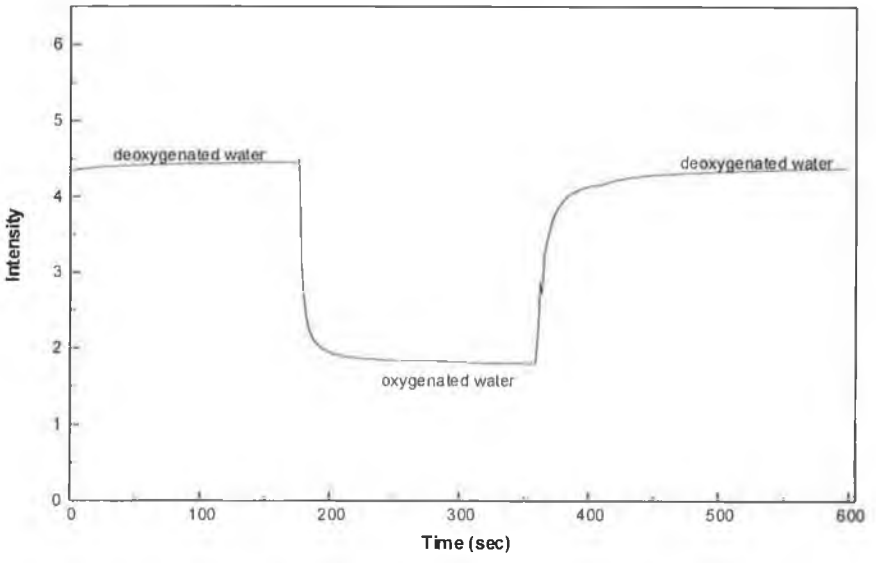

Figure 6.4: Response of a single-sided R=2 MTEOS film in aqueous phase using the prototype system (upside down).

6.4: Version 2 of the Prototype Sensor

The implementation of version 2 of the prototype sensor involved the extension of the previous prototype sensor head to a waterproof dipstick design. A schematic of the mechanical design is presented below in figure 6.5.

Overall the diameter of the sensor head is smaller (approximately 5cm) since surface mount electronics were used for both the LED driver and the photodiode detection circuits. The PCBs used are approximately 4 cm in diameter.

Testing of this version of the prototype was carried out in aqueous phase and the results are shown in figure 6.6. It must be noted that since this version of the prototype was designed and constructed prior to the completion of testing version 1, the problems encountered with the flow cell design persisted. Hence, as before with version 1, the instrument was turned upside down.

Once again the quenching response was found to be reproducible and consistent with that obtained for the same film in the laboratory-based system.

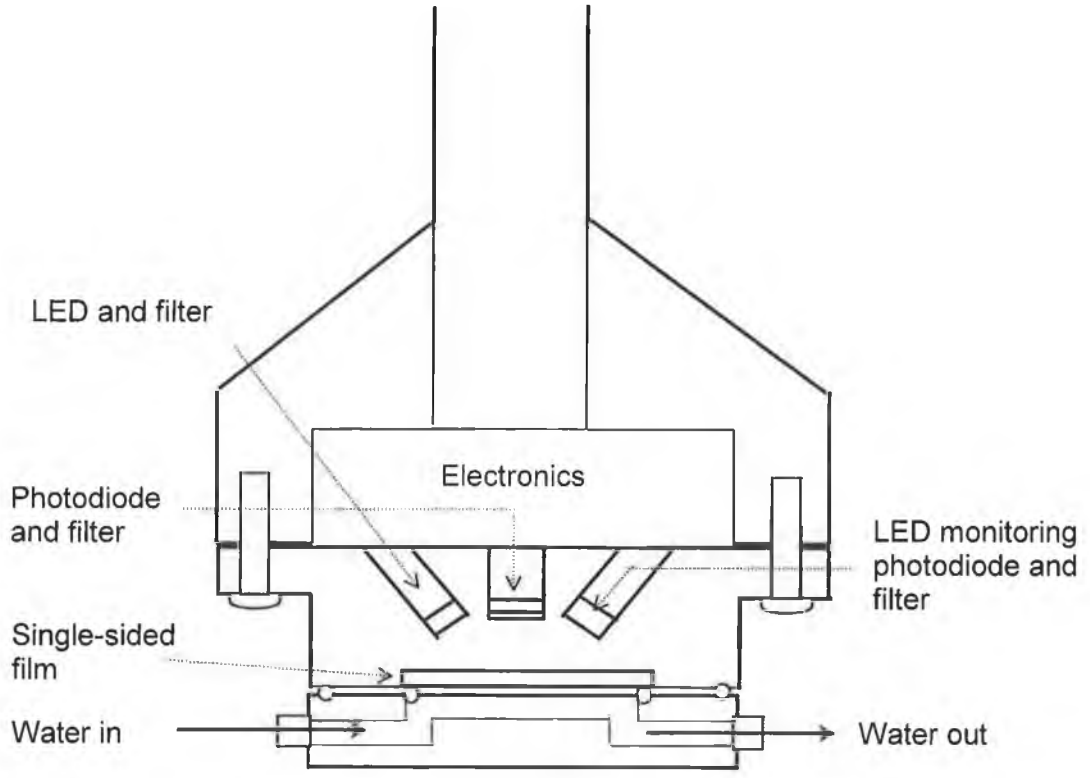

Figure 6.5: Prototype dipstick sensor head with flow cell.

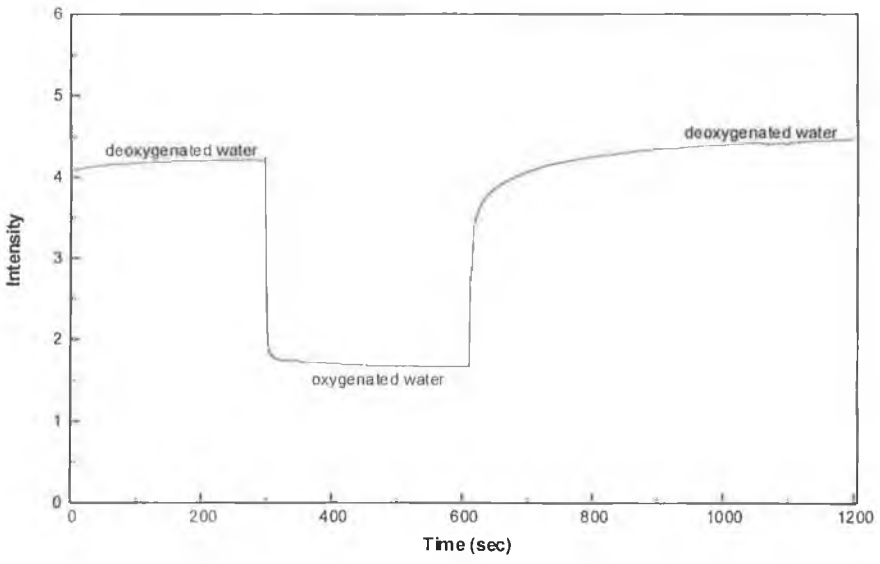

Figure 6.6: Response of single-sided R=2 MTEOS film in aqueous phase using version 2 of the prototype system (upside down).

The response and recovery times for this system were calculated and were found to be 13sec and 146sec respectively. While the response times are fairly consistent with those obtained for version 1, the recovery times are significantly greater. It is thought that these anomalous recovery times may be due to lateral diffusion effects. Looking at figure 6.7 below it can be seen that the sol-gel film coats most of the glass substrate. However, only a small portion (a circle less than 1cm in diameter) of this sensing film is exposed to the excitation light and the flowing water solutions. Hence it is thought that while the oxygen is quickly removed from the circular area of the film when deoxygenated water is flowed through the sensor head, the remaining part of the film effectively acts as a tank of oxygen which slowly diffuses to the centre. The film is slow to fully deoxygenate, giving rise to longer recovery times. The length of these recovery times should be dependent upon the size of the films used, with larger films giving rise to longer recovery times.

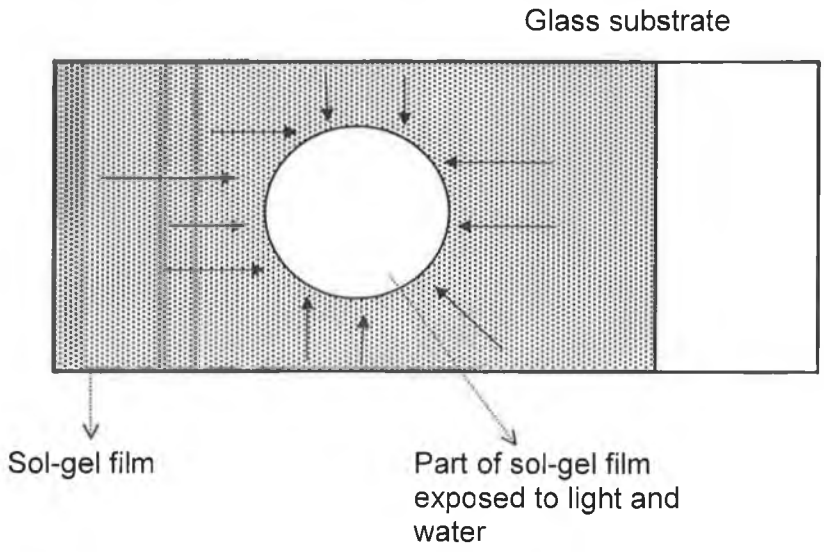

Figure 6.7: Schematic of sample slide used in the prototype systems.

One way to resolve the diffusion problem is to only coat the area of the glass substrate that is exposed to the excitation light and the water. This would mean small circular films of diameter approximately 1cm, possibly spray-or spin-coated onto the glass.

As previously mentioned the use of the flow cell with the dipstick sensor is purely for characterisation purposes. A second cap for the sensor head was designed to allow the sensor to function as a dip probe rather than a flow probe. A schematic of this can be seen in figure 6.8. A hole through the middle of this cap allows water to access the film when the probe is dipped into a sample of water. The use of this probe highlights an important issue, namely the effect of ambient light on the effective operation of the sensor.

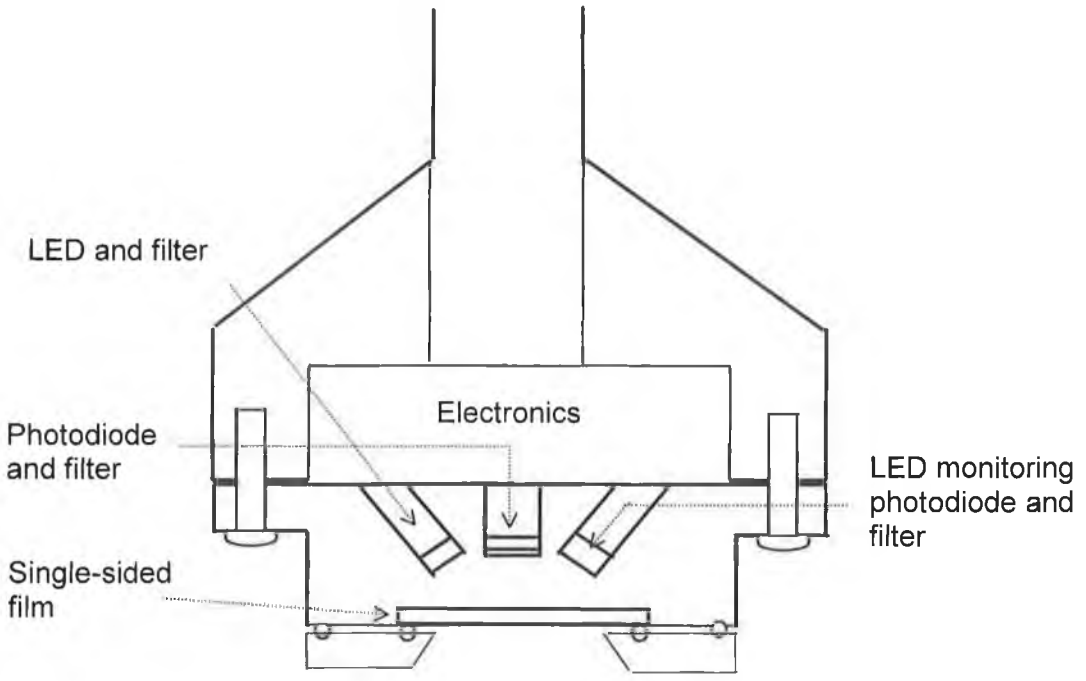

Figure 6.8: Prototype dipstick sensor head – dip-probe version.

With the implementation of the dip probe shown in figure 6.8, clearly it is easier for ambient light levels to be detected by the photodiode and cause incorrect readings. Also there is the possibility that blue LED light could cause various species in a water sample in the field to fluoresce, again causing spurious readings by the photodiode. In order to overcome this it was proposed to coat the sensing film with an opaque barrier layer. A black silicone rubber layer was deemed ideal for this purpose. As discussed previously in chapter 5, the rubber layer is an effective way of maintaining the long term stability of the sensing film by helping to minimise any leaching effects and also preventing bio-fouling of the sensing film.

However the advantage of using a black silicone rubber layer lies in the fact that the black layer is opaque and so provides optical isolation by preventing any ambient light from reaching the photodiode. The coating also prevents the blue LED light from escaping the confines of the sensor head. Full details regarding the development, characterisation and optimisation of the black silicone rubber layer are provided in the next chapter.

Preliminary testing of the dip probe sensor without the flow cell emphasised the problems already encountered with the flow cell. It was found that when the probe was dipped into a sample of water, an air pocket in the cap prevented the water from reaching the sensing film. A similar problem was encountered in versions 1 and 2 with the flow cell. The trapped air at the film surface was obviously related to the mounting of the sensing film at the bottom of the probe. Clearly this hindrance to the effective operation of the sensor was undesirable, and prompted the need to modify the sensor design. The modifications are described in the next section.

6.5: Version 3 of the Prototype Sensor

In an effort to overcome the problem of the air pocket at the film/water interface, it was decided to investigate the feasibility of positioning the sensing film on the side of the dip probe sensor. Consequently, the sensor head was redesigned and constructed as shown in figure 6.9.

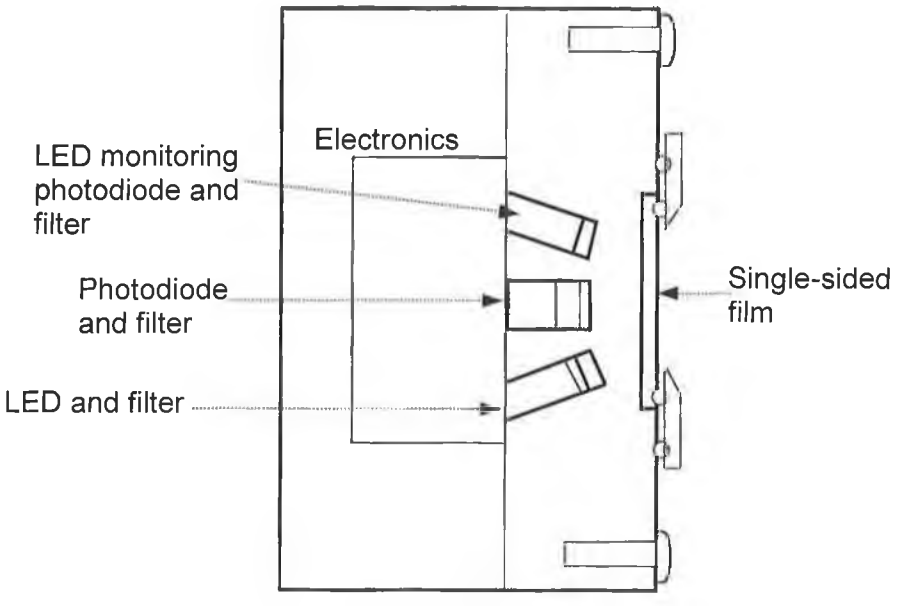

Figure 6.9: Prototype sensor head – Version 3.

From the diagram it is clear that the sensing film was placed in a vertical position on the side of the dip probe. It was thought this would prevent the air pocket when the probe was dipped into a sample of water. All other aspects of the sensor remained as before for version 2.

Once again in order to characterise the performance of this sensor a small flow cell was designed to fit over the film. Preliminary testing of this instrument was carried out in gas-phase using a single sided R=4 MTEOS film. Both oxygen gas and nitrogen gas were alternately flowed through the flow cell. The response of the sensor was recorded and is shown in figure 6.10.

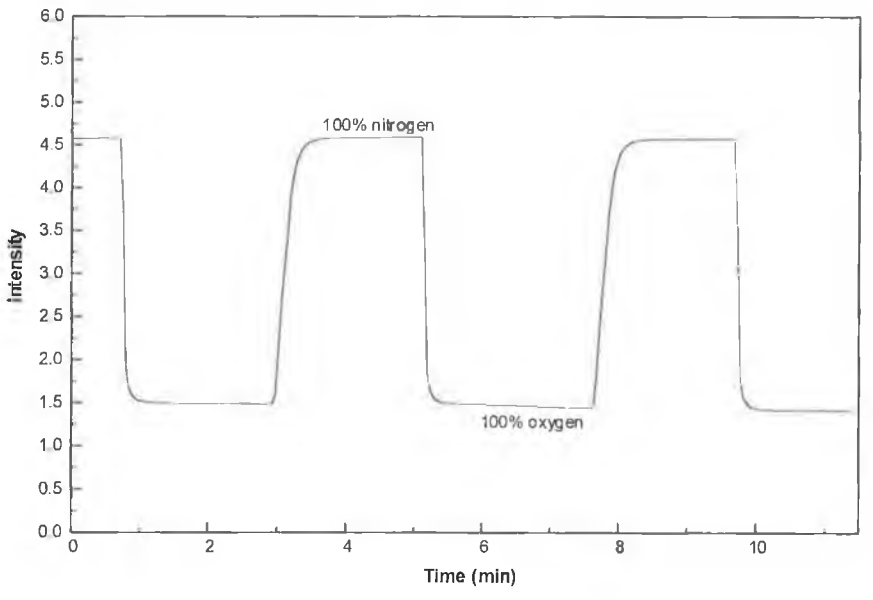

Figure 6.10: Response of single-sided R=4 MTEOS film in gas-phase.

The initial results obtained using this dip probe sensor were very promising. The data above show a good signal to noise ratio, fast response times, and a quenching response of 83%.

The next step in the characterisation of this instrument was the extension of the testing to aqueous phase. The results are shown in figure 6.11. It must be noted that during this experiment some difficulties with the flow cell were encountered. Hence it was necessary to empty the cell each time prior to flowing the deoxygenated or oxygenated solutions.

Consequently, the results in figure 6.11 are not an accurate depiction of the response and recovery times of the sensor.

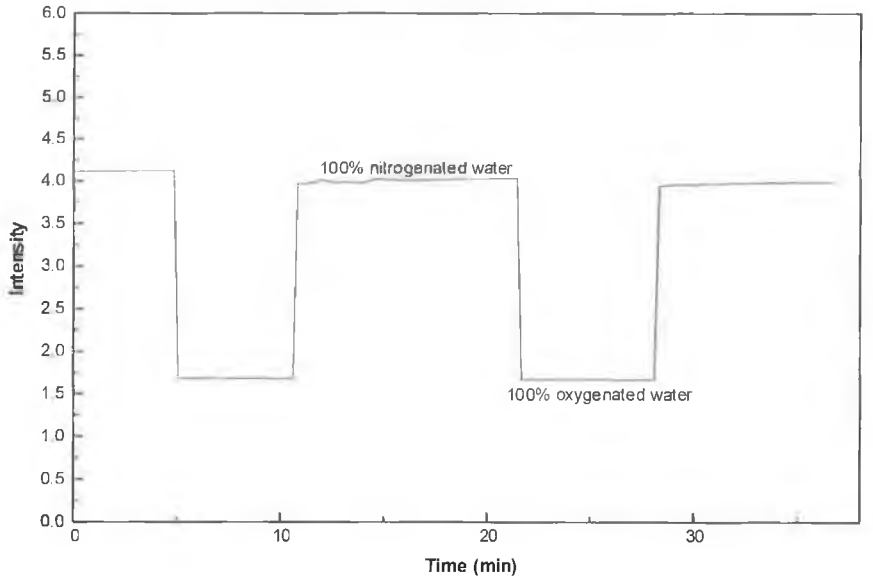

Figure 6.11: Response of single-sided R=4 MTEOS film in aqueous-phase.

Once again the good signal to noise ratio is apparent, and the quenching response was found to be 68%, comparable with results obtained previously. Overall the results were promising.

The next stage is the testing of this sensor as a dip probe whereby the probe is dipped into various solutions of water and its response measured. Ideally, this testing should be carried out with sensing films coated with the optimised rubber coating discussed in the next chapter, to ensure optical isolation. Unfortunately this testing was beyond the scope of this thesis, but is being carried out by colleagues in this laboratory.

6.6: Summary

This chapter traced the development of a prototype dissolved oxygen sensor suitable for field-testing. The primary objective was the production of a compact, dip probe sensor. Altogether three versions of the prototype were developed with each version incorporating new improvements. To date version 3, with the side-mounted film is the most promising. Future work on the prototype design are discussed in chapter 9.

Chapter 7: Characterisation and Optimisation of Silicone Rubber Layer

7.1: Introduction

The previous chapter highlighted the importance of the provision of a suitable optical isolation barrier layer for the sensing films. The use of a silicone rubber coating has been shown to be effective in minimising any leaching effects thus enhancing the long-term stability of the films [1]. However, the developments in the prototype oxygen sensor discussed in chapter 6 heightened the need for a barrier layer that can provide optical isolation to the sensing film. It was proposed that a black silicone rubber layer could fulfil these two roles, since the opaque coating would prevent ambient light from reaching the photodiode, while at the same time act as a barrier layer to minimise leaching as before, and also prevent fouling of the sensing film. Additionally, silicon rubber is one of the most oxygen permeable polymers currently available. This suggests that the additional coating over the sensing film is unlikely to affect its quenching response.

This chapter traces the characterisation and optimisation of the black silicone rubber layer. The effect of the coating on the sensing film performance was fully investigated and is also documented in this chapter.

7.2: Characterisation of Sensing Films

Since the dissolved oxygen prototype developed used single-sided films, it was decided to use them for the purposes of this investigation. Each of the single-sided sensing films was fully characterised in terms of its response to dissolved oxygen, both prior to and after being coated with the black silicone rubber. This involved measuring the quenching response together with both the response and recovery times of the films. These parameters are vital in order to establish whether the rubber coating impinges on the effective operation of the sensing films.

7.2.1: Quenching Response

In order to evaluate the quenching response, the sensing films were alternately exposed to fully oxygenated and fully deoxygenated water solutions as described in chapter 4. It must be noted that these characterisations were carried out using the laboratory-based sensor shown in figure 4.1. The results were recorded and the quenching response was calculated using equation 4.1:

$$Q_{DO} = \frac{I_{deoxy} - I_{oxy}}{I_{deoxy}} \qquad (4.1)$$

Where, I_{deoxy} is the fluorescence intensity in the presence of fully deoxygenated water and I_{oxy} is the fluorescence intensity in the presence of fully oxygenated water.

7.2.2: Response and Recovery Times

The response time of the sensing film is defined as the time it takes for the intensity in totally deoxygenated water to change to that in fully oxygenated water. This parameter is effectively a measure of the turn-on time of the sensor. The recovery time is the time taken for the intensity in fully oxygenated water to change to that in fully deoxygenated water or the turn-off time of the sensor. Figure 7.1 shows the response of a single-sided R=2 MTEOS film in aqueous phase. From this graph it is evident that the recovery time is considerably longer than the response time. This hyperbolic quenching response is characteristic of the sensing films and is treated in detail by Mills *et al* [2]

Throughout this work the response times are described in terms of t_{90}. This is the time it takes for the signal to drop to 90% of the full-scale value for response time, and the time it takes to rise to 90% of the full-scale value for recovery time [3.].

As previously mentioned, all characterisation of the films was carried out using the laboratory-based system. Hence all response and recovery times quoted later in this chapter include the fill-time of the 9ml characterisation cell and the delivery time of the calibrated solutions to the sensing substrate within the cell, and so are not the true response and recovery times of the sensing films. However, since the parameters are required for comparison purposes only, the true times are not necessary.

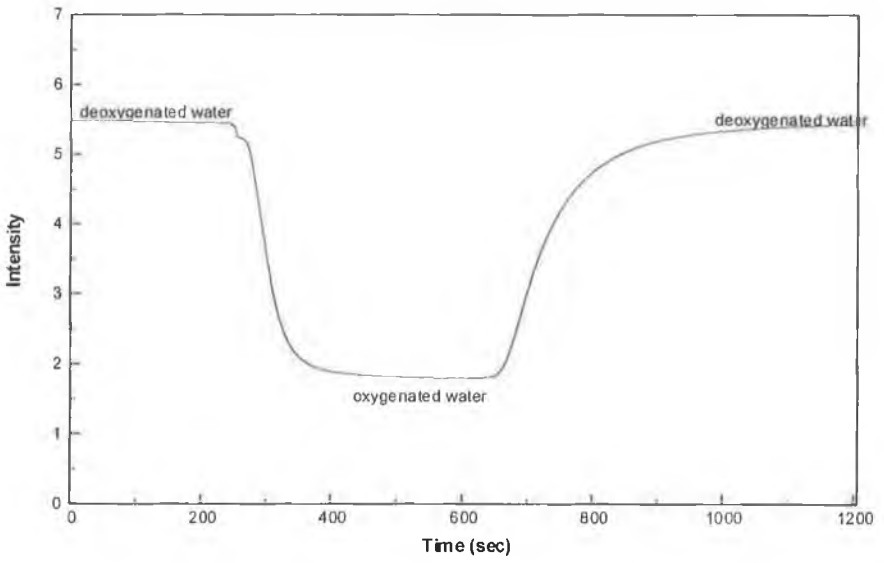

Figure 7.1: Response and recovery of a single-sided R=2 MTEOS film.

7.3: Black Rubber Coatings

Two different types of black silicone rubber were used to fabricate the barrier layers. The first was Dow Corning Sylgard 170. This consists of two parts, the black base component (part A) and the curing agent (part B), which are mixed together in equal proportions. At a later stage in the project an improved compound was identified.

The most important feature of the black silicone rubber coating is the thickness. It is essential that the coating is thick enough to maintain its colour and hence its opacity. However it must not be too thick as to interfere with the successful operation of the sensing film by altering the quenching response or the response times. In order to fabricate a range of coatings of varying thickness, a solvent was chosen for each black rubber. For the Sylgard 170 hexane was chosen and a number of solutions of the black rubber in hexane were fabricated and coated onto the sensing films. Similarly for the Wacker rubber, the solvent toluene was found to be the most suitable.

7.4: Dow Corning Sylgard 170

Initially, a single-sided R=2 MTEOS film was chosen and its response to dissolved oxygen characterised. The uncoated side of the film was masked and an undiluted layer of the black rubber was dip-coated onto the film using the apparatus shown in figure 2.2. The rubber coating was then left to cure for approximately three days. Once cured the coated sensing film was re-characterised to establish the effect if any on the film operation.

The response of the film, both before, and after the coating with rubber can be seen in figures 7.2 and 7.3. Although there was no difference in the quenching response with Q_{DO}=70% in both cases, the difference in response times of both films is clearly visible. The response time was found to increase from 93sec to 420sec and the recovery time increased from 164sec to 817sec. This was clearly unacceptable and thought to be due to the thickness of the film, which was measured to be approximately 300μm. Hence in order to overcome this, different solutions of varying amounts of black rubber in hexane were made up and dip-coated onto some single-sided R=2 MTEOS films.

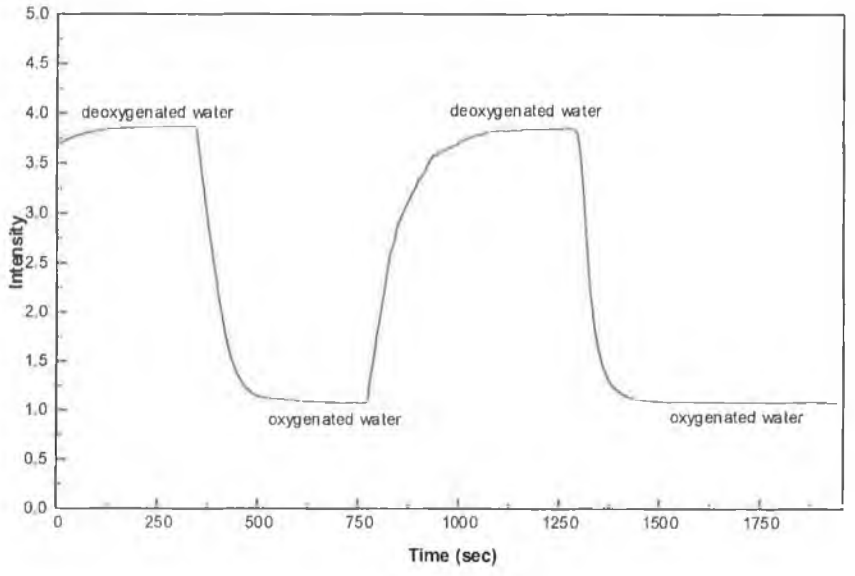

Figure 7.2: Response of single-sided R=2 MTEOS film in aqueous phase before coating with Sylgard 170.

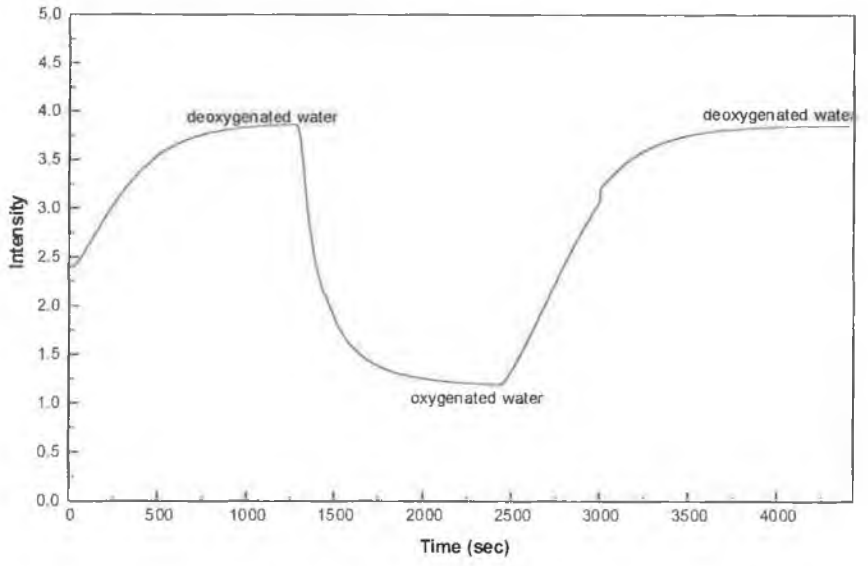

Figure 7.3: Response of single-sided R=2 MTEOS film in aqueous phase after coating with Sylgard 170.

As before, each of the films was characterised both before and after coating with silicone rubber. Tabulated below in table 7.1 are the quenching responses of each of the coated films, measured before and after coating with the Sylgard 170. Clearly the addition of the barrier layer had no effect on the film's quenching response which concurs with expectations. However, the rubber coating did have a noticeable effect on the response and recovery times. For the most part an unacceptable increase in the response and recovery times was observed. This is evident from the data in table 7.2.

% w/w black silicone rubber in hexane:	Quenching Response (%) ± 2%:	
	Before coating:	After coating:
100	70	68
80	70	69
60	68	69
50	70	70

Table 7.1: Quenching response of R=2 MTEOS films before and after coating with Sylgard 170.

% w/w black silicone rubber in hexane:	Response time:(sec)		Recovery time: (sec)	
	Before	After	Before	After
100	93	420	164	817
80	69	132	208	340
60	118	101	204	229
50	71	94	213	327

Table 7.2: Response and recovery times of R=2 MTEOS films before and after coating with Sylgard 170.

The data above highlights the problem of placing a barrier layer over the sensing films. The oxygen takes longer to diffuse through the coating to access the fluorescing ruthenium complex, resulting in the longer response and recovery times. This was verified by monitoring the response of the film coated with the undiluted rubber to gas-phase oxygen, shown in figure 7.4. In this case the response and recovery times increased to 16sec and 53sec respectively. This is particularly slow for gas-phase detection given the fact, that sub-second times are normally recorded for sol-gel films not coated with rubber [4.].

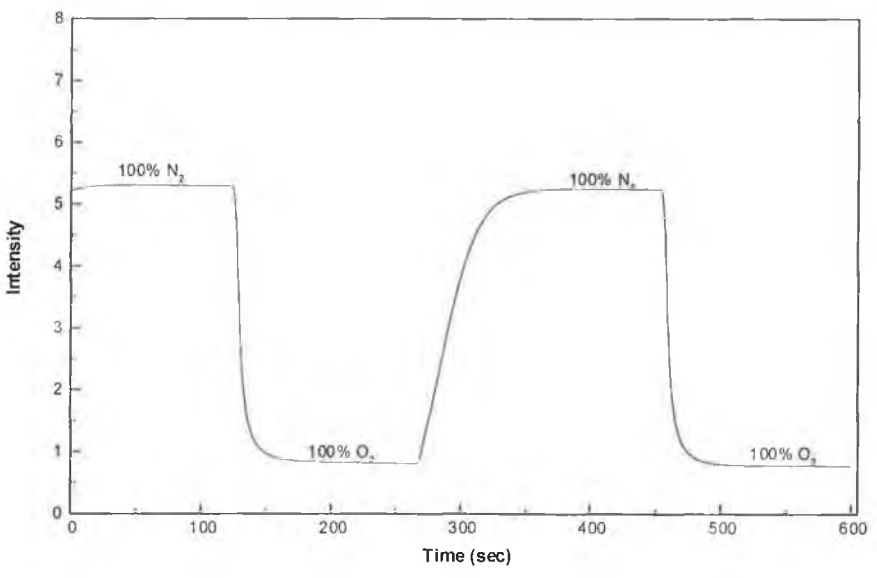

Figure 7.4: Response of single-side R=2 MTEOS film in gas-phase after coating with Sylgard 170.

Another reason for the increase in response and recovery times is the type of black rubber used, namely Sylgard 170. This rubber contains carbon, which attributes the black colour to the carbon. However carbon is known to absorb gases including oxygen, and it is thought that this may be occurring in the coating [5]. Hence, the absorption of the oxygen by the carbon inhibits the sensing mechanism and increases the observed response and recovery times.

7.4.1: Transmission Characteristics

The transmission spectra of each of the films were examined over the visible range from 400nm to 700nm using a Shimadzu UV/VIS spectrophotometer. The purpose of this was to determine if the rubber effectively blocks all ambient light. This optical isolation of the sensing films is essential given the design of the prototype sensing system as described later in chapter 8. A summary of the transmission characteristics is provided in table 7.3.

% w/w black silicone rubber in hexane:	% Optical transmission @ 400nm-700nm:
100	0
80	1-3
60	20-40
50	65-75

Table 7.3: Transmission characteristics of single-sided R=2 MTEOS films coated with Sylgard 170.

From the data above it is apparent that the film coated with the undiluted black rubber is the only viable option for use in the sensing system since it is the only film that prevents the transmission of ambient light. However the increase in response and recovery times when the films are coated with this type of rubber is obviously unsatisfactory and requires resolution. Moreover, these films were difficult to coat onto the sensing films and adhesion was not good. Once coated, the films tended to peel off very easily. Hence it was proposed that another black silicone rubber be tried.

7.5: Wacker N189:

Communication with other researchers in related areas indicated that the black silicone rubber, Wacker N189 might be suitable for the purposes of this project. After some trial and error it was found that 62% w/w black rubber in toluene was the optimum solution for use as a barrier layer [6]. The result was a coating, which retained its black colour and hence the ability to block ambient light, but which was thin enough not to effect the response and recovery times of the sensing film too much.

Previously, R=4 MTEOS films were identified as the optimum films for dissolved oxygen sensing due to a lack of leaching. Hence a number of single-sided R=4 MTEOS films were coated with the black rubber solution with full characterisation carried out both before and after coating.

The responses of one of these films to dissolved oxygen, before and after coating with the rubber are shown in figures 7.5 and 7.6.

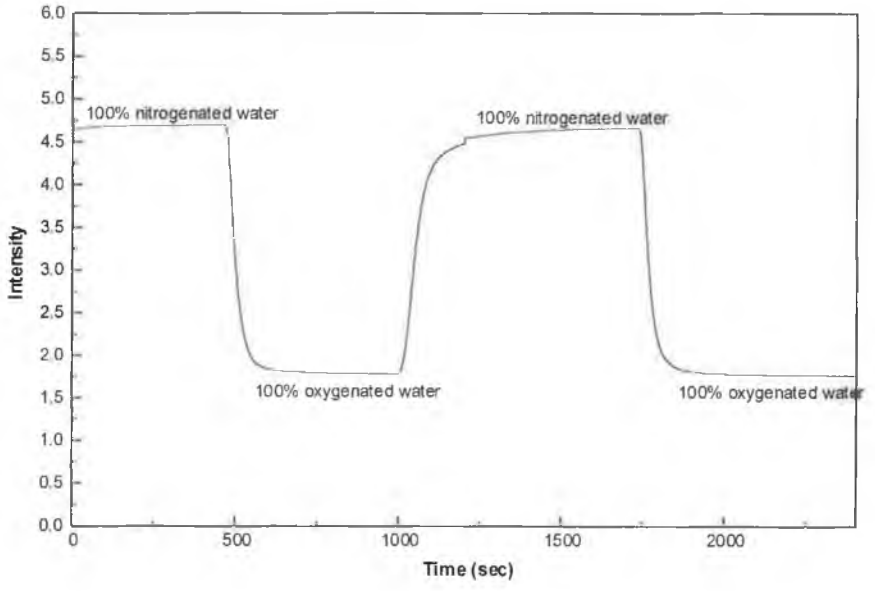

Figure 7.5: Response of single-sided R=4 MTEOS film in aqueous phase before coating with Wacker N189.

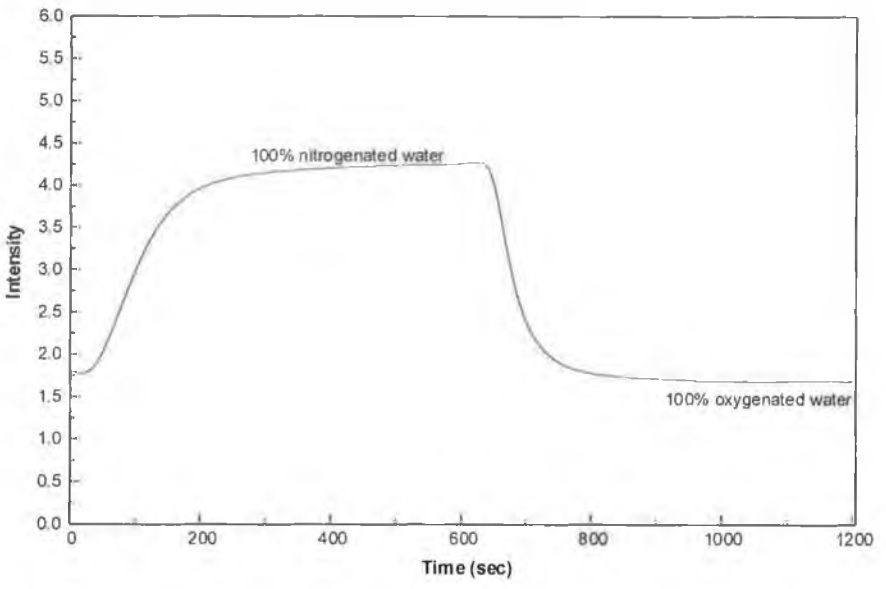

Figure 7.6: Response of single-sided R=4 MTEOS film in aqueous phase after coating with Wacker N189.

The films coated with Wacker N189 proved superior to those coated with Sylgard 170 despite an increase in the response and recovery times. The response time was found to increase from 62sec to 93sec and the recovery time was found to increase from 121sec to 164sec. It must be noted that these increases are less than those measured for the films coated with Sylgard 170, primarily due to the fact that the Wacker rubber coatings are much thinner, with a average measured thickness of 30μm [6.]. The quenching response, Q_{DO}, was also calculated and found to be 61% in both cases. However, perhaps the most promising characteristics of the Wacker coatings were the film quality and transmission characteristics. The overall quality of the films was good and the films adhered well to the substrates. Additionally, these black rubber coatings transmitted no visible light when tested using a spectrophotometer.

7.6: Summary

This chapter traced the characterisation and optimisation of a black silicone rubber layer for the purposes of optical isolation of the sensing film, the minimisation of any leaching effects, and the prevention of bio-fouling of the sensing film. Two different black rubber compounds were tested. The Wacker N189 proved the most promising since it did not impinge upon the effective operation of the sensing films, and provided the best optical isolation.

References:

[1.] C. M. McDonagh, A. M. Shields, A. K. McEvoy, B. D. MacCraith, J. F. Gouin; **Optical Sol-Gel-Based Dissolved Oxygen Sensor: Progress Towards a Commercial Instrument,** *J. Sol-Gel Sci. Technol.,* 1998, Vol. 13, pp. 207-211.

[2.] A. Mills, Q. Chang; **Modeled diffusion-controlled response and recovery behaviour of a naked optical film sensor with a hyperbolic-type response to analyte concentration,** *Analyst,* 1992, Vol. 117, pp. 1461.

[3.] A. K. McEvoy; **Development of an Optical Sol-Gel-Based Dissolved Oxygen Sensor**, PhD Thesis, 1996, Dublin City University, (unpublished).

[4.] Personal communication with Dr. Jean-Francois Gouin, Optical Sensors Laboratory, Dublin City University.

[5.] Personal communication with Dr. Chris Malins, Optical Sensors Laboratory, Dublin City University.

[6.] Michael Niggeman, Optical Sensors Laboratory, Dublin City University, unpublished results.

Chapter 8: Temperature Dependence of Sensing Films

8.1: Introduction

This chapter documents the investigations carried out to establish the temperature dependence of the optical dissolved oxygen sensor under development. It is important that the exact nature of this dependence be established since it impinges on all aspects of the sensor performance. In particular, the long-term stability of the calibration cannot be established and the effective operation of a calibration protocol would prove impossible until the sensor response is temperature compensated.

8.2: Temperature Dependence of Sensor Performance

There are two contributing factors to the temperature dependence, namely, the temperature dependence of the fluorescence intensity and that of the quenching response. The temperature dependence of the absolute fluorescence intensity is related to the change in fluorescence quantum efficiency with temperature. This manifests itself as a change in fluorescence lifetime. The fluorescence lifetime is defined as the average period of time a fluorophore remains in the excited state prior to its return to the ground state. As the temperature increases, the non-radiative decay rate (the inverse of the lifetime) increases, giving rise to a corresponding increase in the observed decay rate according to the following equation:

$$\frac{1}{\tau_{obs}} = \frac{1}{\tau_{rad}} + \frac{1}{\tau_{non-rad}} \qquad (3.1)$$

Where, $1/\tau$ is equal to the decay rate, k, and where obs., rad., and non-rad., refer to the observed, radiative, and non-radiative lifetimes respectively.

Hence, increasing the temperature results in decreased observed lifetimes arising from increased non-radiative decay rates caused by the decrease in quantum efficiency [1,2]. A resulting decrease in absolute fluorescence intensity occurs with increasing temperature.

The temperature dependence of the quenching response, Q_{DO}, is more complex. It has previously been proposed in chapter 4, that the operation of this dissolved oxygen sensor is based on the principle whereby the oxygen partitions out of the water at the film/water interface and accesses the dye complex in gas-phase. The hydrophobic nature of the MTEOS films used for this study is clearly conducive to this process, although the gas partitioning is not 100% efficient. Hence, the relative contribution to the fluorescence quenching by both gas-phase and aqueous phase oxygen in the pores must be considered.

The temperature dependence of the quenching is primarily influenced by the variation of the oxygen diffusion coefficient with temperature. In particular, an increase in temperature results in an increase in the diffusion coefficient and hence an increase in the quenching response.

The temperature dependence of the quenching response coupled with the temperature dependence of the fluorescence intensity constitutes the overall temperature sensitivity of the dissolved oxygen sensor.

8.3: Gas-phase Temperature Dependence

As mentioned in the previous section, in gas-phase, the variation of the oxygen diffusion coefficient with temperature governs temperature dependence of the quenching response. In an effort to demonstrate this, the following experiment was carried out. A schematic of the system used is shown in figure 8.1.

Initially, nitrogen gas was circulated through the characterisation cell, which housed both the sensing film and a temperature probe. The sensing film used was a R=2 MTEOS film. Both the cell and its contents were heated up with a hot air blower, and the output from the sensor was monitored and recorded.

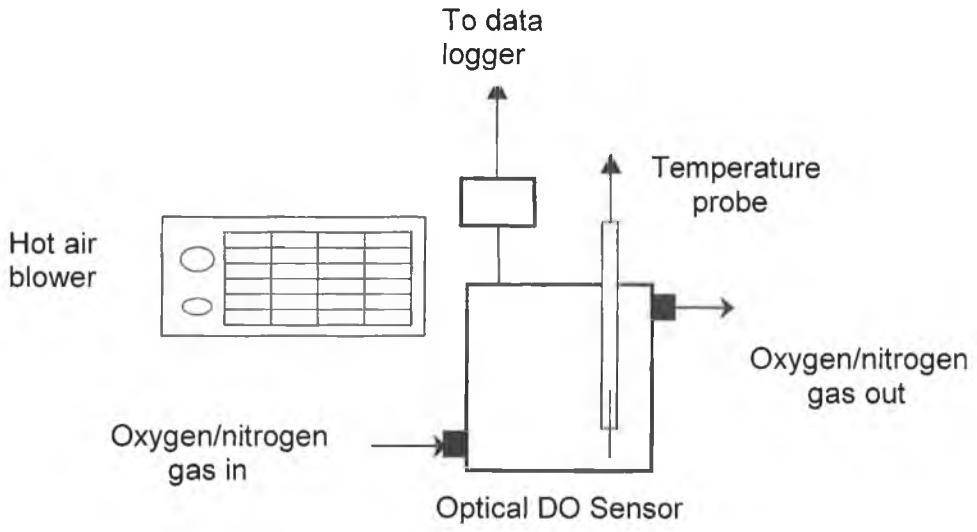

Figure 8.1: System for gas-phase temperature dependence.

The resulting plot of intensity as a function of temperature, in the absence of oxygen, is shown in figure 8.2. The procedure was repeated for a 100% oxygen environment, the results of which are also presented in figure 8.2.

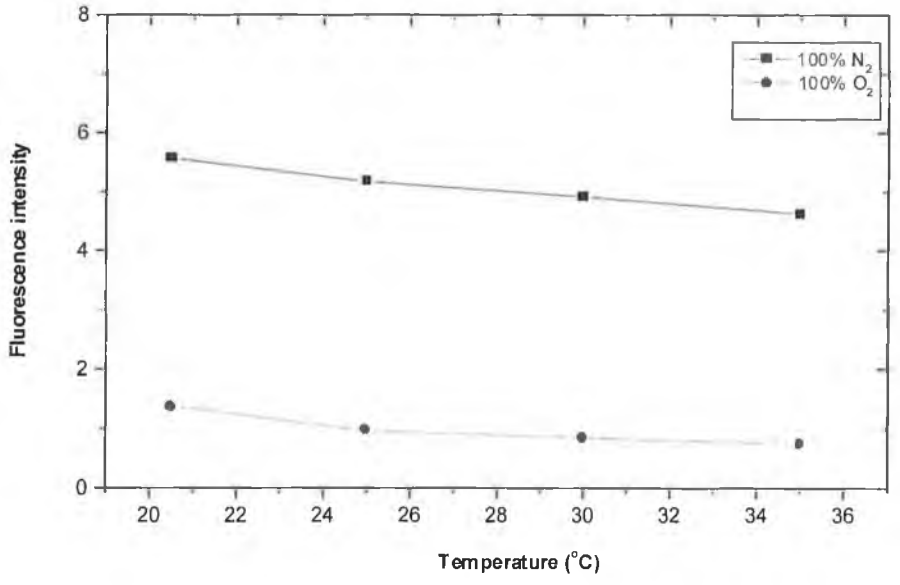

Figure 8.2: Temperature dependence of the fluorescence intensity in both 100% O_2 and 100% N_2 gas.

A plot of the resulting gas-phase quenching response, Q_G, versus temperature is shown in figure 8.3. Clearly this experiment, although crude, confirms the expected temperature dependence of the gas diffusion coefficient in the sensing film. The plot below shows an increase of 9% in the gas-phase quenching response corresponding to a 15^0C rise in the temperature. It must be noted that this gas-phase experiment was difficult to carry out due to the difficulty in achieving and maintaining a constant gas temperature. It was predicted that the experiment would be easier in aqueous phase.

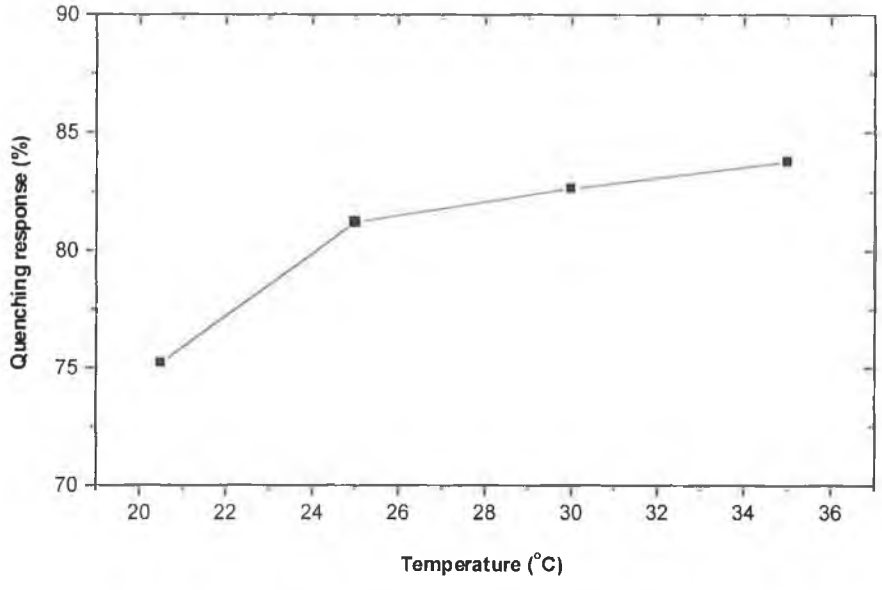

Figure 8.3: Temperature dependence of overall gas-phase quenching response, Q_G.

8.4: Aqueous-phase Temperature Dependence

A similar investigation to that detailed above was carried out to determine the aqueous-phase temperature dependence of a R=2 MTEOS film. These studies were carried out using the system shown in figure 8.4.

In this case, solutions of oxygenated and deoxygenated water were heated using the heater on the magnetic stirrer, and were then circulated through the measurement cell, which housed the sensing film and the temperature probe. The outputs from both the optical dissolved oxygen sensor and the temperature probe were connected directly to a data logger which enabled the respective responses to be sampled simultaneously every 8 seconds during the course of the experiment.

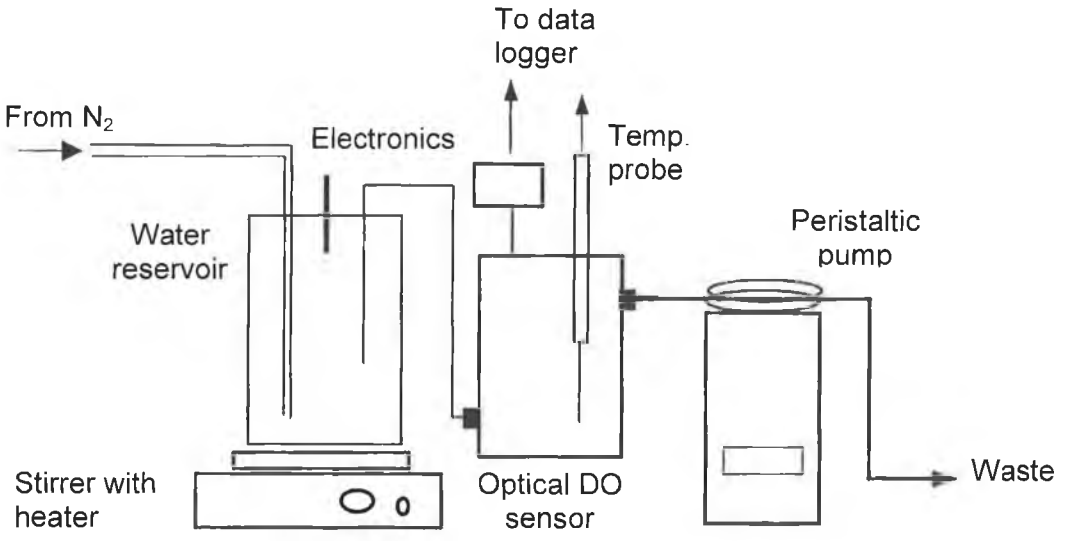

Figure 8.4: System for aqueous-phase temperature dependence.

Intensity as a function of temperature was recorded for both deoxygenated and oxygenated water and the resulting quenching response, Q_{DO} versus temperature was calculated from the data. The data are plotted in figures 8.5 and 8.6.

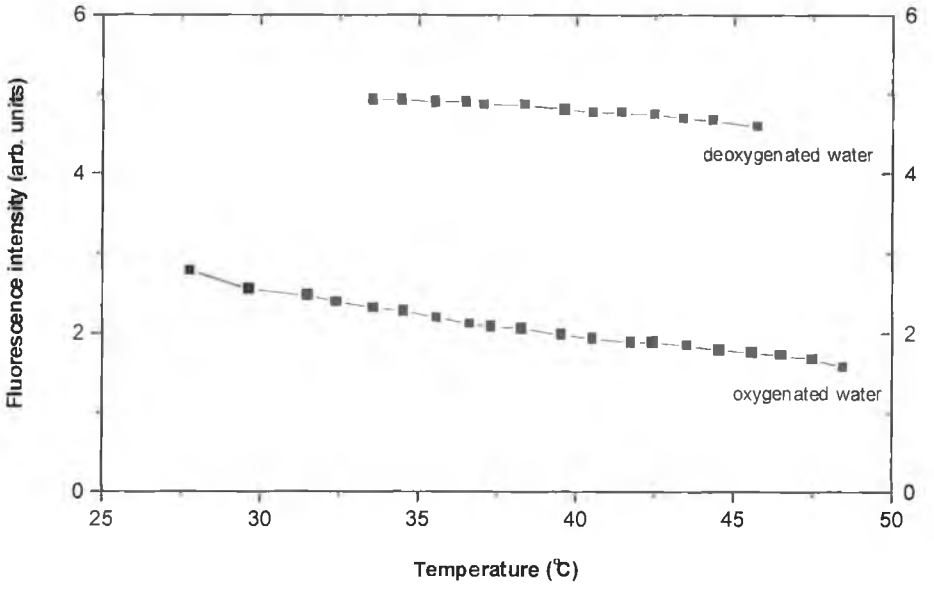

Figure 8.5: Temperature dependence of the fluorescence intensity in both oxygenated and deoxygenated water.

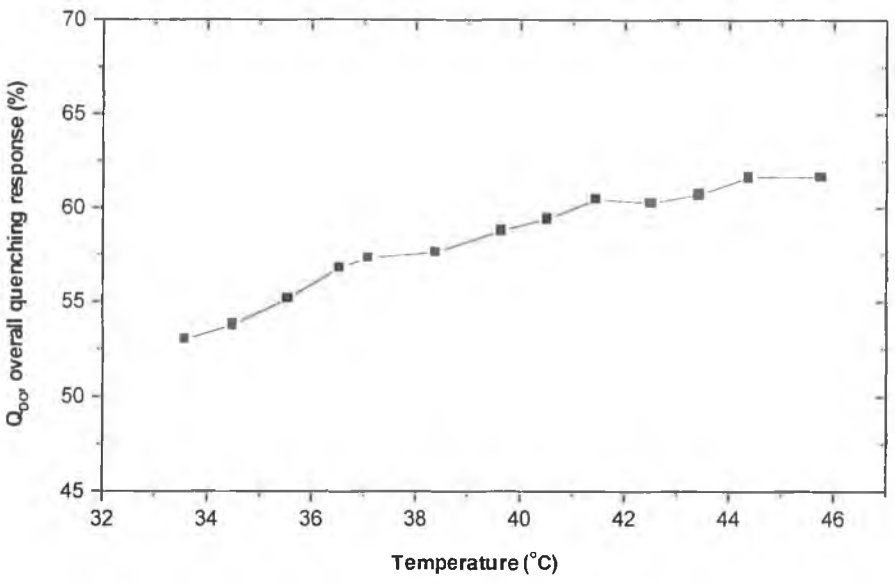

Figure 8.6: Temperature dependence of overall aqueous phase quenching response, Q_{DO}.

The data presented in the above figures show both a decrease in the absolute fluorescence intensity and an increase in the quenching response as a function of increasing temperature, as previously predicted. However, much difficulty was encountered in trying to achieve a consistent trend for the same film. The intention was to characterise film performance over the temperature range 10-40°C. However, the system used was rather crude and it was difficult to reproduce water temperatures accurately. Hence it was decided to use a sensing system developed by colleagues, which could be immersed in a temperature-controlled bath. Further details regarding this system, the experiments carried out, and the results obtained are provided in the next section.

8.5: Temperature Dependence System

8.5.1: Planar Waveguide Oxygen Sensor

Recently, colleagues developed a sensing system for both gaseous and dissolved oxygen [3]. A schematic of this system is shown in figure 8.7. A blue LED is used as an excitation source and is placed at normal incidence under the sensing slide. These sensing films are single-sided and fabricated as before.

The fluorescence, emitted in the sensitive sol-gel layer, is coupled into the slide, which acts as a waveguide, is detected by a photodiode, which is placed at an angle θ to the end-face of the substrate. A small amount of the blue LED light is coupled into the slide by scattering. However, the fluorescence collected at the end-face is strongly angular dependent, whereas the blue light coupled into the slide is not. Thus, by positioning the photodiode at the optimum output angle, the proportion of blue light arriving at the photodiode is small enough to enable good sensing performance.

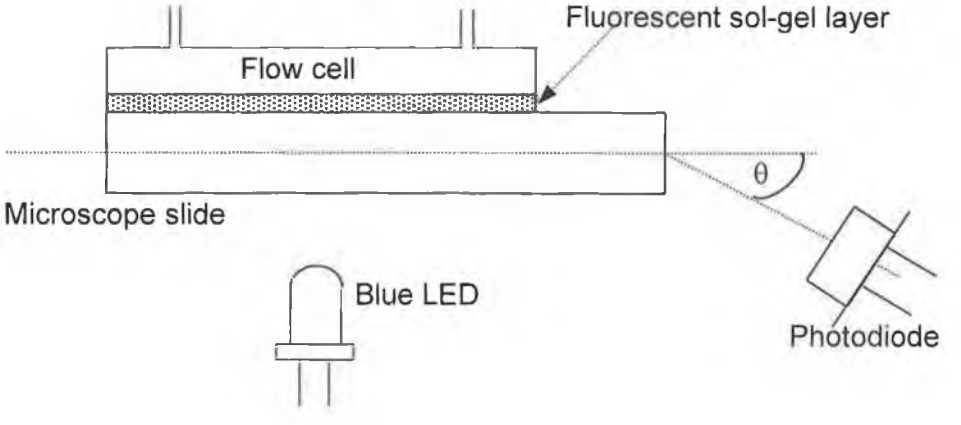

Figure 8.7: Planar waveguide oxygen sensor.

Each of the elements shown in figure 8.7 were housed together in a sensor head approximately 4cm in diameter. This sensor head was used in the experimental arrangement, described in the next section, for the determination of the temperature dependence. The compact nature of the sensor head meant it could be immersed into the constant temperature bath unlike the sensor used in previous experiments.

8.5.2: Experimental System

The experimental arrangement used to establish the temperature dependence is shown in figure 8.8. The sensor head was placed into a small vessel into which calibrated solutions of oxygenated water were flowed. The vessel itself was immersed in a constant temperature bath and a temperature sensor was located close to the sensing film.

For each temperature the sensor responses to 0, 10, 20, 30, 40, 50, 60, 80, and 100% oxygenated water were recorded. In effect, the corresponding calibration curve was recorded for each temperature. This was repeated for each of the temperatures, 10°, 15°, 20°, and 25°.

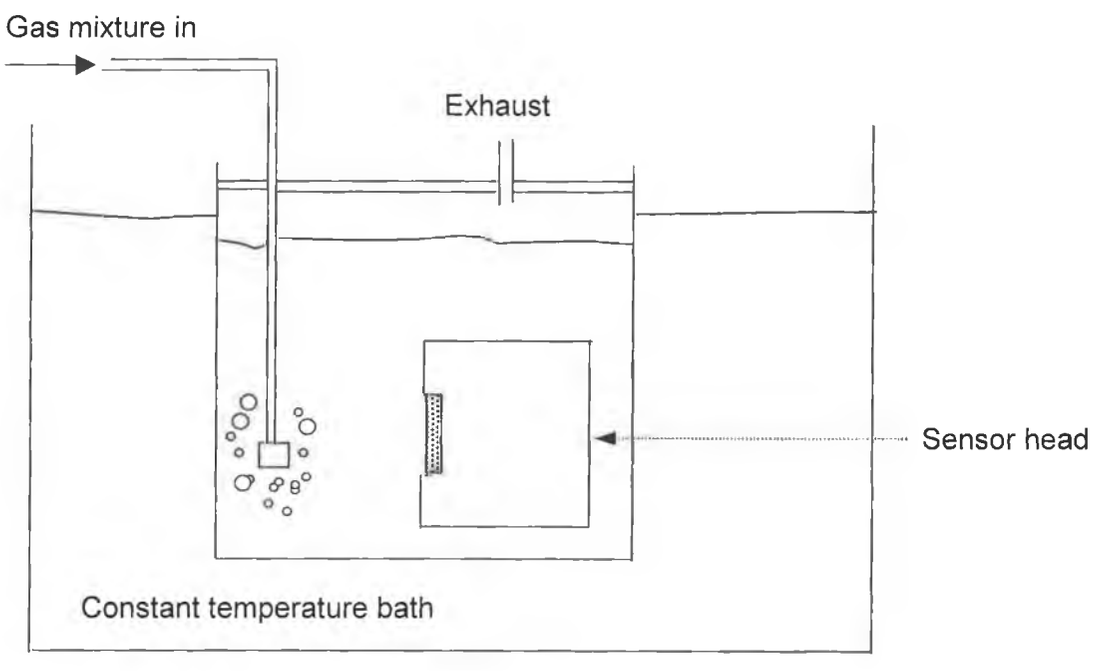

Figure 8.8: Temperature dependence experimental system.

8.6: Temperature Dependence of the Dissolved Oxygen Sensor

The calibration curves of a R=4 MTEOS film in aqueous phase for five different temperatures were obtained using the system described in the previous section. Figure 8.9 shows the corresponding plots of intensity versus oxygen concentration for each of these temperatures. Clearly, as predicted there is a decrease in the fluorescence intensity with temperature.

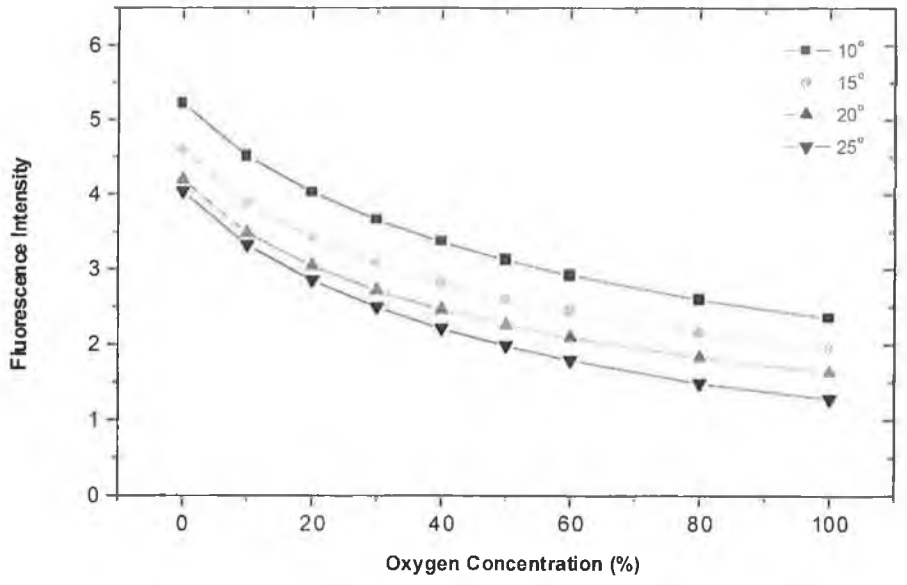

Figure 8.9: Fluorescence intensity as a function of temperature.

A corresponding plot of quenching response as a function of temperature is shown in figure 8.10. As predicted an overall increase, of approximately 8%, in the quenching response was recorded over the temperature range from 10°C to 25°C.

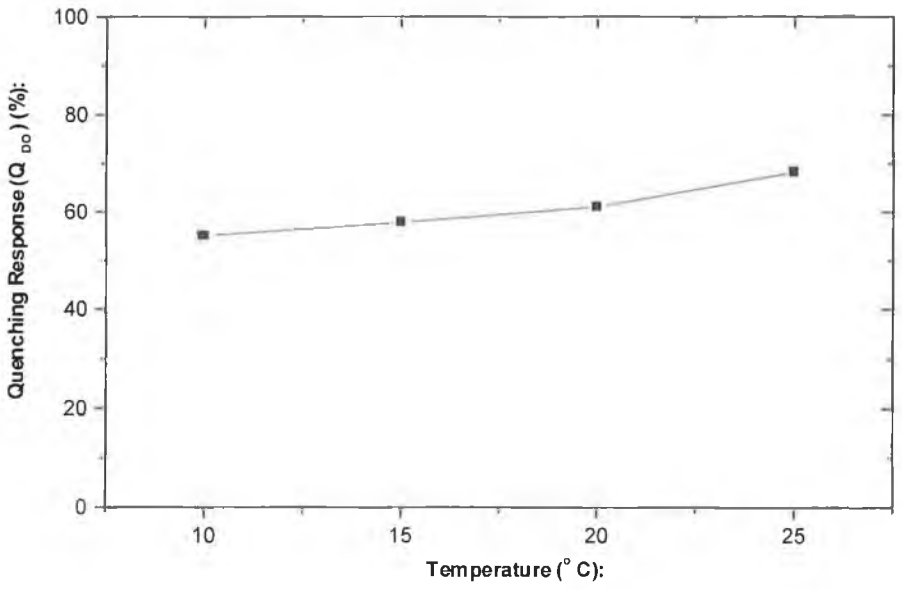

Figure 8.10: Quenching response as a function of temperature.

8.7: Summary

This chapter detailed the investigation into the temperature dependence of the dissolved oxygen sensor. A full description of the theoretical contributions and behaviours was provided. Preliminary methods in both gas-phase and aqueous phase, although crude, gave results in agreement with those predicted. A more accurate method of determining the temperature dependence involved the use of a constant temperature bath. Results obtained were again in agreement with theory, and the predicted overall increase in the quenching response with increasing temperature was observed.

At this point my contribution to the sensor development ended and the project was handed over to another researcher. However, the next step in the development of the commercial sensor is to use the results obtained above in order to generate a temperature compensation algorithm and incorporate it into the sensor data acquisition software.

References:

[1.] N. Opitz, H. J. Graf, D. W. Lubbers; **Oxygen Sensor for the Temperature Range 300 to 500K based on Fluorescence Quenching of Indicator-Treated Silicone Rubber Membranes,** *Sensors and Actuators,* 1988, Vol. 13, pp. 159-163.

[2.] J. N. Demas, B. A. DeGraff; **On the design of Luminescence based Temperature Sensors,** *Proc. SPIE,* 1992, Vol. 1796, pp. 71-75.

[3.] J. F. Gouin, A. Doyle, B. D. MacCraith; **Fluorescence capture by planar waveguide as platform for optical sensors,** *Electronics Letters,* 1998, Vol. 34, no. 17, pp. 1685-1687.

Chapter 9: Conclusion

9.1: Overall Summary and Conclusions

The investigation into the sensing film stability comprised a study of both leaching and photobleaching effects. The optimum fabrication conditions were established, in order to eliminate dye leaching. No photobleaching effects were detected in the sol-gel films used throughout this study. The long-term stability of the calibration function was also investigated. This study indicated that the film microstructure slowly evolves to produce a denser film, over a period of months, thus decreasing the oxygen sensitivity of the films. This effect requires further investigation.

The need for optical isolation of the sensing films was established, and the use of a black silicone rubber coating for this purpose was investigated. In all, two different types of rubber compound were used and the coated film response times and transmission characteristics were optimised for optimum sensor performance.

The contributions to the temperature dependence of the sensing films were discussed and a number of different experimental configurations were used to measure this dependence. The data obtained was consistent with theoretical predictions.

Finally, a series of three prototype dissolved oxygen sensors were designed and tested. The design modifications required to move from the existing laboratory test environment to a practical field-testing environment were detailed. Problems with the first two designs were identified and modifications made for version 3 of the prototype, which yielded satisfactory dissolved oxygen quenching data.

At this point my contribution to the dissolved oxygen sensor development ended and other researchers took over the work.

9.2: Future Work

As stated above, a different research team is continuing the prototype development. Although the design of version 3 discussed in chapter 6 overcomes many of the difficulties associated with the previous designs, problems remain to be solved. These include difficulty with sensor film insertion reproducibility, electronic baseline instability, and temperature drift.

Additionally, as discussed previously, problems with the long-term stability of the sensor films needs to be addressed. Finally, a more comprehensive temperature dependence investigation needs to be carried out in order to generate a temperature correction algorithm for the sensor.

9.3: Objectives Revisited

Overall the project objectives stated in section 1.6 have been achieved. Good progress was made with the prototype design and testing. However, more work is required to achieve a commercially viable sensor. Also, more extensive temperature dependence investigations are required. Unfortunately, due to time constraints this work was beyond the scope of this thesis.

9.4: List of Publications and Conference Presentations

Poster Presentations:

"Optimisation of sol-gel-derived silica films for optical oxygen sensing"
The Institute of Physics Optical Group*: Optical Sensing and its Applications*
Nov. 13th, 1996, DIT, Kevin Street.

"Development and optimisation of an optical sol-gel based dissolved oxygen sensor"
IOP, Irish Branch, Spring Weekend Meeting
21-23 March, 1997, Donegal.

Oral Presentations:

"An optical sol-gel based dissolved oxygen sensor: progress towards a commercial instrument" - presented by supervisor.
Enviro Sense '97: *Chemical, Biochemical, and Environmental Sensors IX*
June 16-20, 1997, Munich, Germany

Publications:

Optical sol-gel-based dissolved oxygen sensor: Progress towards a commercial instrument, Journal of Sol-Gel Science and Technology, Vol. 13, pp. 207-211 (1998)

Appendix 1: Prototype Electronics Circuitry

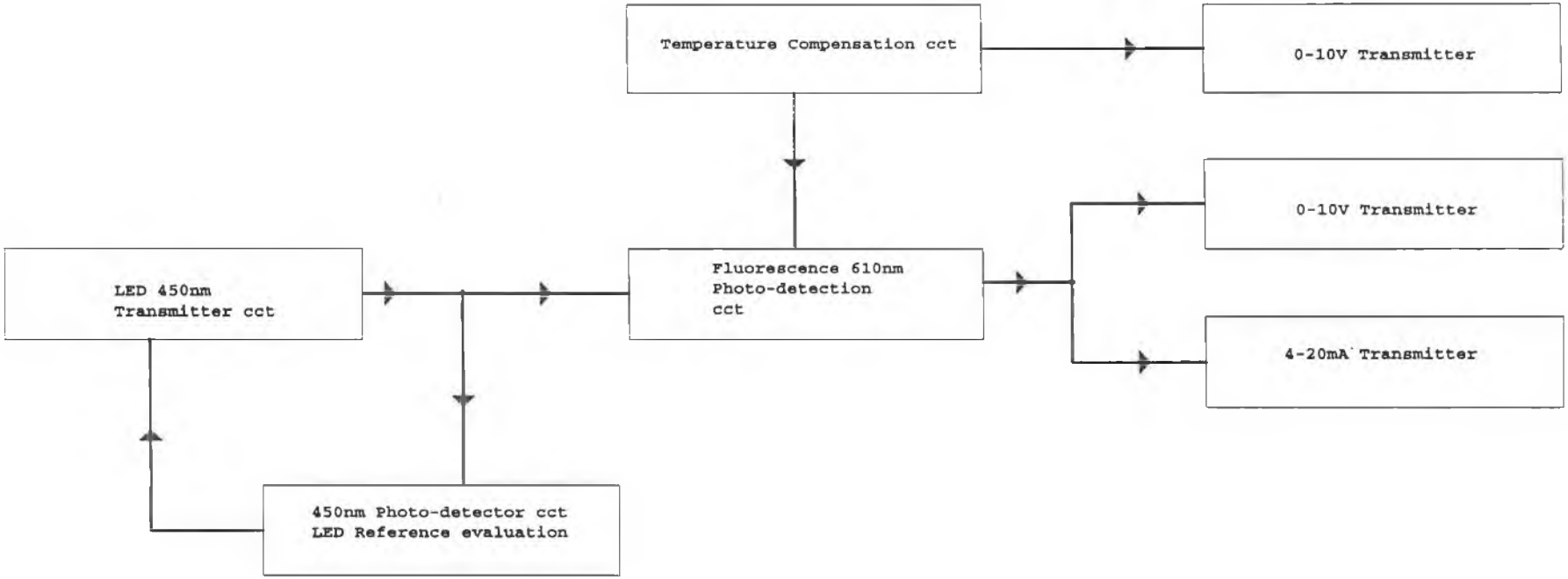

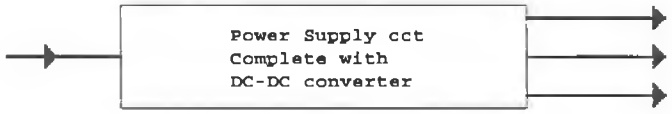

PEI Technologies Dublin City University		
System Block Diagram		
A3	Project DC97008	2
Monday, July 14, 1997	1	5

Power Supply Circuit

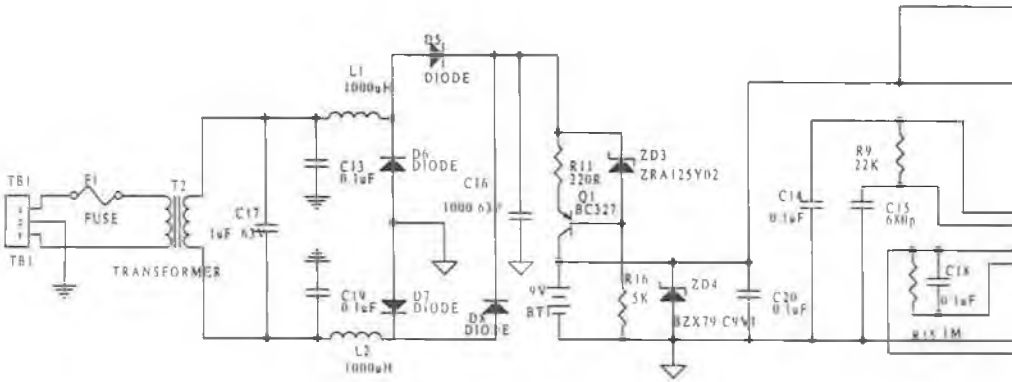

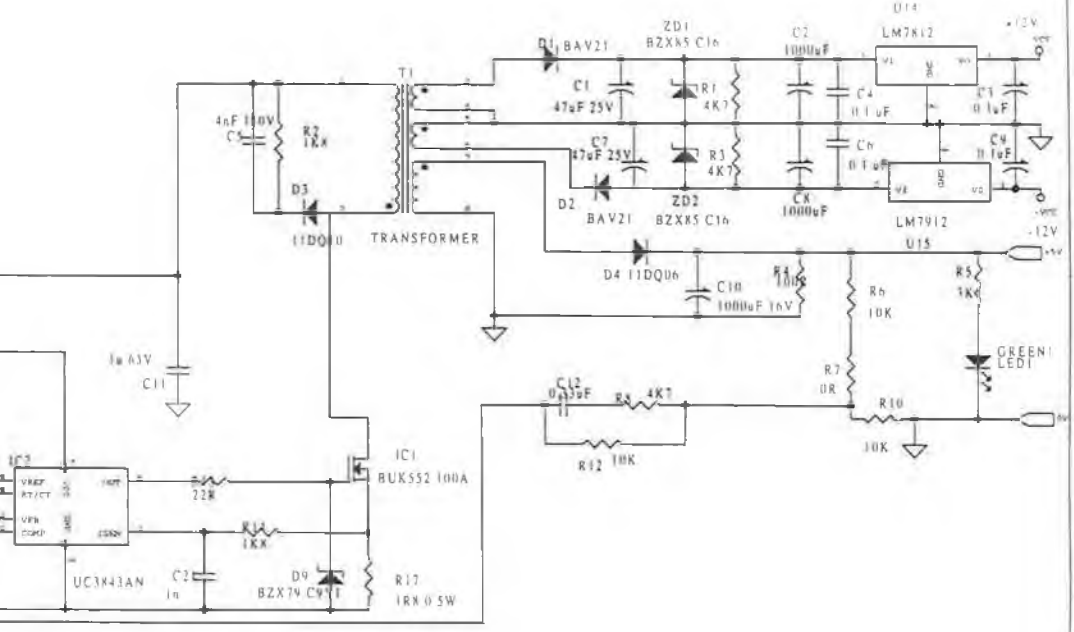

Power Supply Circuit		
A3	Project DC97008	2
Tuesday, July 15, 1997		

Transmitter

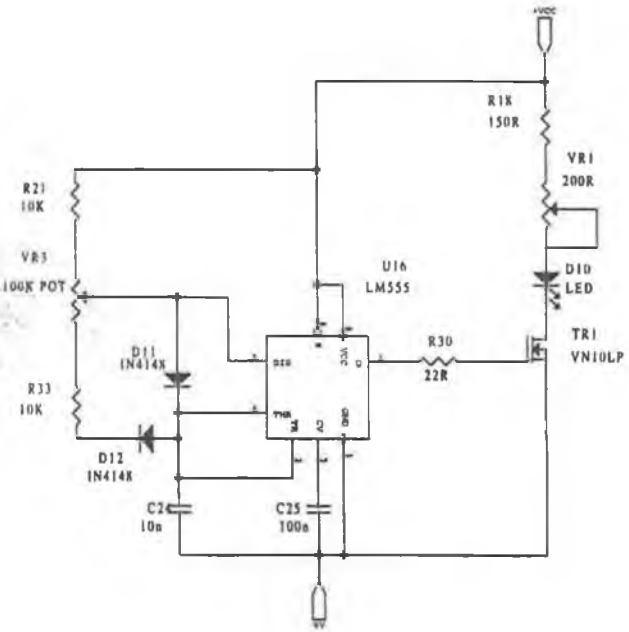

0V

0-10V Input

4-20mA OUTPUT

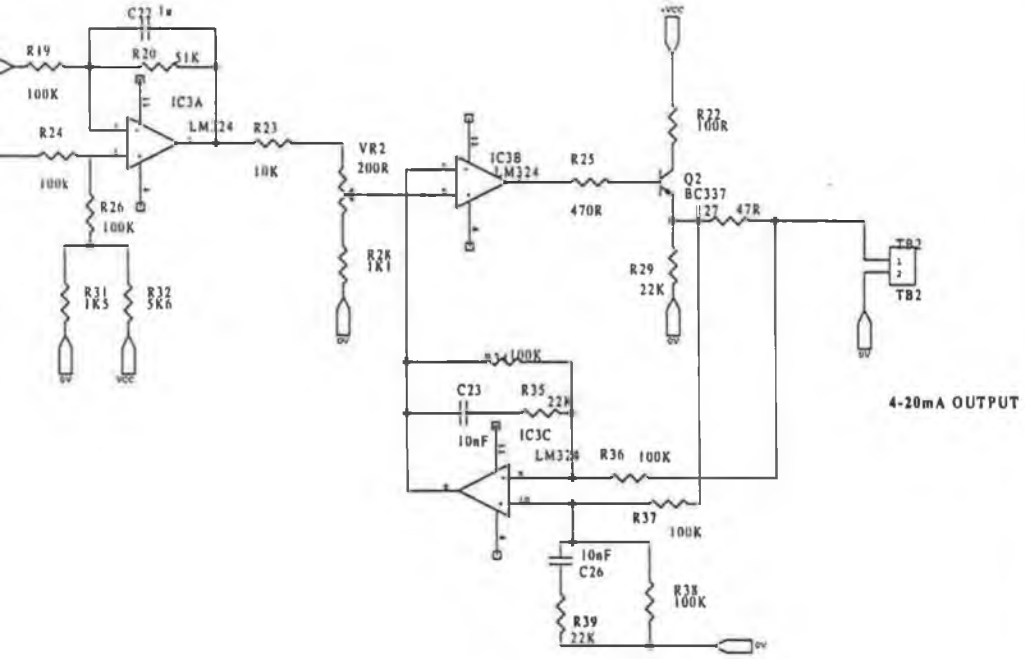

Transmitter and 4-20mA Output Circuits		
A3	Project DC97008	2
Monday, July 14, 1997	1	5

Receiver

610nm Fluorescence Detector

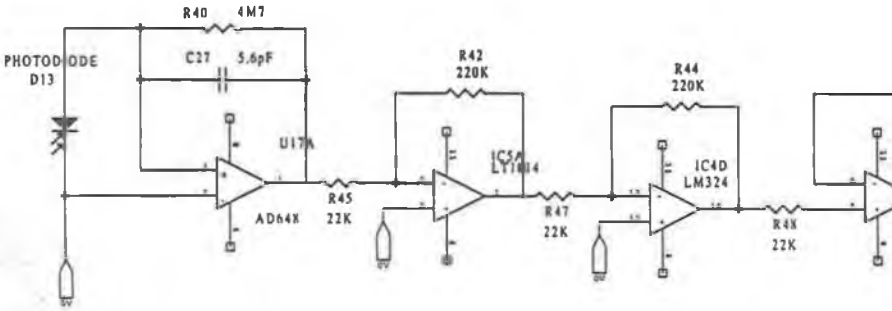

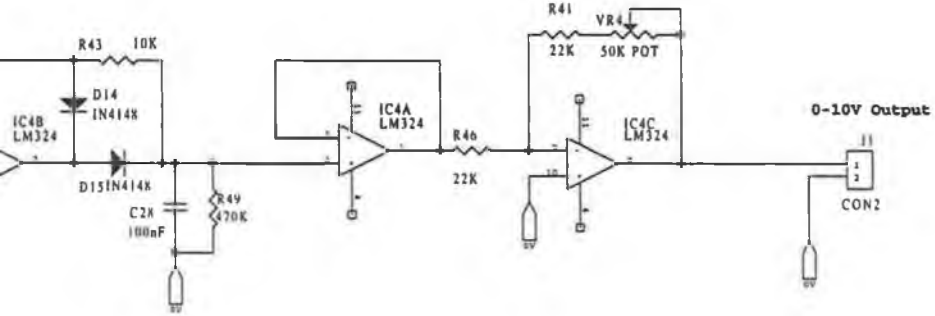

610nm Dectection and 0-10V ccts		
A3	Project DC97008	2
Monday, July 14, 1997	4	5

Receiver

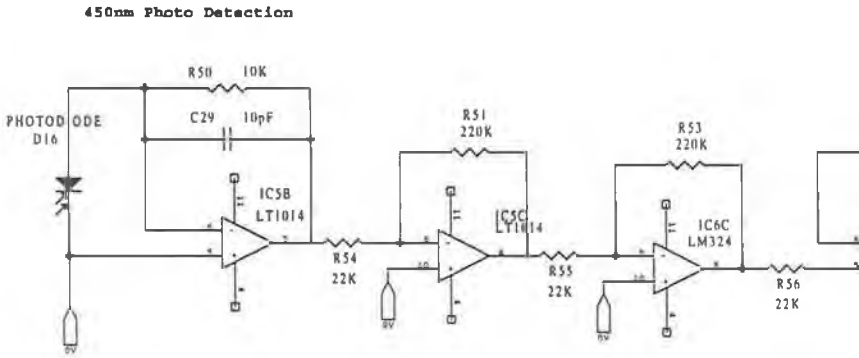
450nm Photo Detection
R50 10K
PHOTOD ODE
D16
C29 10pF
IC5B
LT1014
R54
22K
R51
220K
IC5C
LT1014
R55
22K
R53
220K
IC6C
LM324
R56
22K

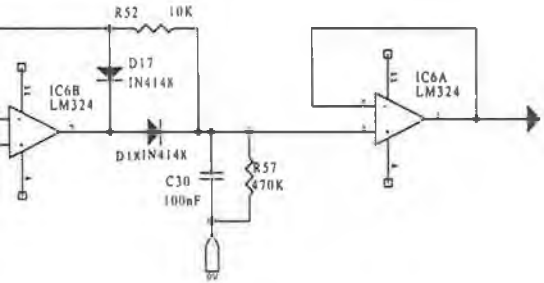

450nm Detection Circuit		
A3	Project DC97008	2
Monday, July 14, 1997	5	5